# A NOVEL APPROACH FOR FABRICATION OF SINGLE SILICON/SILICON OXIDE NANOPILLARS AT PRECISE LOCATIONS

by

SRAVAN CHOWDARY TALASILA

Presented to the Faculty of the Graduate School of

The University of Texas at Arlington in Partial Fulfillment

of the Requirements

for the Degree of

MASTER OF SCIENCE IN

MATERIAL SCIENCE AND ENGINEERING

THE UNIVERSITY OF TEXAS AT ARLINGTON

DECEMBER 2016

Copyright © by Sravan Chowdary Talasila 2016

All Rights Reserved

# Acknowledgements

I would like to express my immeasurable appreciation and deepest gratitude for everyone who has been behind me helping out in one way or another in making this study possible.

First, I would like to thank my thesis advisor, Dr. Seong Jin Koh for his support, advice, guidance, valuable comments, suggestions, and provisions that benefited me in the completion of the thesis. Without his guidance and persistent help, this work would not have been possible.

I am extremely thankful to my peer member Manouchehr, who shared many lectures regarding the project and helping me out with the experiments. I would like to thank Shahab in guiding and assisting me through my work. I would extend my gratitude to all professors and staffs in the department of Materials Science and Engineering and NanoFAB Research Center for having their support and encouragement.

I have to thank Dennis Bueno, Kevin Chambers, Huan Nguyen and Nader Hozhabri for granting me access to NanoFAB Research Center and helping me out in processing equipment's which are needed in the fabrication of silicon wafer.

I extend my gratitude to committee members, Dr. Yaowu Hao and Dr. Kyungsuk Yum for having their time in reviewing my thesis defense.

Finally, I have to thank my family and friends who had extended their support and encouragement for my study at UTA.

This work was supported by National Science Foundation (CMMI-1463451).

November 16, 2016

Abstract

A NOVEL APPROACH FOR FABRICATION OF SINGLE SILICON/SILICON OXDIE NANOPILLARS AT PRECISE LOCATIONS

Sravan Chowdary Talasila, MS

The University of Texas at Arlington, 2016

Supervising Professor: Seong Jin Koh

Nanopillars exhibit novel electrical and optical properties which could not be obtained from bulk materials. Many of their practical applications would require controlled placement of nanopillars at exact locations. However, precise placement and large scale fabrication of nanopillars have been challenging with conventional fabrication techniques. This thesis investigates a new approach to fabricate nanopillars at exact locations on a large scale. In this approach, fabrication of nanopillars is accomplished by first placing nanoparticles (NP) at exact locations and then performing anisotropic dry etching using these NPs as hard masks, resulting in formation of nanopillars on exact substrate positions. Precise placement of nanoparticles was carried out by forming an electrostatic guiding template that forces nanoparticles onto site specific locations on the substrate. The electrostatic guiding template was made of a gold layer on $SiO_2$ substrate in which 100nm circular holes are made with underlying $SiO_2$ substrate exposed. The gold substrate surface and exposed $SiO_2$ surface were functionalized with self-assembled monolayers of 16-mercaptohexadecanoic acid (MHA) and 3-aminopropyltriethoxysilane (APTES), producing negatively and positively charged surfaces, respectively. DNA-functionalized Au nanoparticles (negatively charged due to DNA) were used for the nanoparticle hard masks. Guiding of the DNA-functionalized Au nanoparticles to a specific location was conducted by using the electrostatic funneling technique, where the SAMs-functionalized template guided the

Au nanoparticles onto center positions of the circular holes. Placement of exactly one single Au nanoparticle at the center of the circular $SiO_2$ exposed area was achieved using self-limiting electrostatic gating, which was controlled by varying ionic and pH concentration of the solution during attachment. Subsequently, with the precise placement of Au nanoparticles, a selective removal of Au deposited layer was carried out, leaving the single Au nanoparticles at specified positions on the $SiO_2$ substrate. Then, using AuNP as a hard mask $SiO_2$ layer was anisotropically etched to form $SiO_2$ nanopillars. Using these $SiO_2$ pillars as etch masks, Si substrate was subsequently etched anisotropically. With the above process, the resultant nanopillars had the lengths of 100 nm and diameter of 30 nm at desired locations. These controlled placements of nanopillars could be potentially used in electrical/ optical devices and chemical/biological sensors.

# Table of Contents

Acknowledgements ..... i

Chapter 1 Introduction ..... 1

1.1 Motivation and Approach ..... 1

1.2 Thesis outline ..... 1

Chapter 2 Background ..... 3

2.1 Fabrication of Nanopillars ..... 3

2.1.1 Nanopillar Fabrication Using Top-Down and Bottom-Up Approaches ..... 3

2.1.2 Nanopillar Fabrication by Controlled Oxidation ..... 5

3.2 Fundamentals of charge carriers ..... 6

3.2.1 Zeta Potential ..... 6

3.2.2 Debye Length ..... 7

3.2.3 Factors Affecting SPP ..... 8

3.2.3.1 DNA ..... 9

3.3 Experimental Background ..... 10

3.3.1 Lithography ..... 10

3.3.1.1 Electron Beam Lithography ..... 11

3.3.2 E-Beam Resist ..... 12

3.3.3 SAM’s Layer ..... 13

3.3.3.1 Amino-Terminated Functional Group on Silicon Oxide Surface ..... 15

3.3.3.2 Carboxyl-Terminated Functional group on Gold ..... 16

3.3.4 DNA-Functionalized Gold Nanoparticles ..... 17

3.3.4.1 DNA ........ 17
3.3.4.2 Functionalizing Au ........ 18
3.3.4.2.1 Effect of Salt Concentration ........ 18
3.3.4.2.2 Effect of Au Nanoparticle Size on DNA Surface Loading ........ 19
3.3.5 Electrostatic Funneling ........ 20
3.3.6 Thermal Oxidation ........ 21
3.3.7 Wet Etching ........ 22
3.3.8 Dry Etching ........ 23
3.3.8.1 What is Plasma? ........ 23
3.3.8.2 Plasma-Them RIE ........ 24
3.3.8.3 Trion Reactive-Ion-Etching ........ 25
Chapter 3 Fabrication Process ........ 27
3.1 Prototype ........ 27
3.2 Experimental Materials ........ 28
3.2.1 Reagents ........ 28
3.2.2 Stock Solutions ........ 29
3.3 Experimental Instruments ........ 29
3.4 Substrate Preparation ........ 30
3.4.1 Si Wafer Cleaning ........ 30
3.4.2 Thermally Deposited $SiO_2$ ........ 31
3.4.2 Sample Cleaning ........ 32
3.4.3 Spin Coat Negative E-beam Photoresist ........ 32

3.4.4 E-Beam Lithography ..... 33
3.4.5 Development ..... 34
3.4.6 Evaporation ..... 34
3.4.7 Lift-off and Cleaning ..... 35
3.5 Single Particle placement ..... 35
3.5.1 Au Conjugate ..... 36
3.5.2 Formation of SAM’s Layer ..... 39
3.5.2.1 Formation of Positive Charge ..... 40
3.5.2.2 Formation of Negative charge ..... 40
3.5.3 Directed Self-Assisted Au Placement ..... 41
3.6 Selective Template Removal ..... 41
3.6.1 Resist Coating ..... 42
3.6.2 UV Curing Flood Lamp ..... 42
3.6.3 Resist Strip ..... 43
3.6.4 Au and Cr Etch ..... 43
3.6.5 Cylindrical Resist Etch ..... 44
3.7 Nanopillar Fabrication ..... 45
3.7.1 Silicon oxide Reactive Ion Etching ..... 45
3.7.1 Anisotropic Silicon Etching ..... 47
Chapter 4 Results and Discussion ..... 50
4.1 Exposure dose ..... 50
4.2 Directed self-assisted Placement ..... 51

4.2.1 Selectivity of Au nanoparticle placement ....................................51

4.2.2 Ion Concentration Effect..............................................................52

4.2.3 pH Effect.......................................................................................53

4.3 Resist Strip ..........................................................................................54

4.4 Selective Template removal................................................................55

4.5 Plasma-Therm RIE...............................................................................56

4.6 DRIE etching ........................................................................................57

4.7 Buffered Oxide Etch ............................................................................62

Chapter 5 Conclusion and Future Prospect............................................................64

References ................................................................................................................66

## List of Illustrations

Figure 1 Fabrication of FET device ........ 4

Figure 2 Processing of nanowire silicon transistor ........ 4

Figure 3 Schematic depiction of fabrication sequence for silicon nanopillar arrays using controlled oxidation a) Photoresist on thermally oxidized silicon wafer b) Photolithography used for a feature size of 500 nm c) Etching oxide film d) Etching into silicon substrate e) Oxidizing Si f) Stripping oxide g) Oxidizing Si h) Stripping oxide [5] ........ 5

Figure 4 Schematic representation of ionic charges around a charged particle in a aqueous media ........ 6

Figure 5 schematic of Debye length ........ 8

Figure 6 Surface density of thiol terminated DNA on 13nm gold nanoparticle as a function of NaCl concentration ........ 9

Figure 7 Surface Modification of SiO2 using APTES [31] ........ 15

Figure 8 Schematic representation of possible orientations of APTES molecules on silicon oxide surface [34] ........ 16

Figure 9 DNA molecular structure [37] ........ 18

Figure 10 DNA loading (# DNA strands/nanoparticle) vs NaCl concentration on 15nm Au nanoparticle [38] ........ 19

Figure 11 Surface density of thiolated ssDNA having $T_{10}$ spacer on 13nm gold nanoparticle as a function of NaCl concentration in the immobilization solution [39] . 19

Figure 12 Mechanism of dry etching [45] ........ 24

Figure 13 Steps involved in the fabrication of device ........ 28

Figure 14 Sample size ........ 30

Figure 15 Bare silicon wafer ........ 31

Figure 16 Thermally deposited silicon oxide ........ 31

Figure 17 E-beam resit coating on silicon oxide ........ 33

Figure 18 E-beam exposed patterns on negative resist ............................................ 33

Figure 19 Developed resist patterns ............................................ 34

Figure 20 Chrome (50nm) and gold (10nm) deposition ............................................ 35

Figure 21 Lift-off process ............................................ 35

Figure 22 Single particle placement ............................................ 36

Figure 23 Working schematics of NAP 5 column [46] ............................................ 38

Figure 24 DNA functionalized Au nanoparticle ............................................ 39

Figure 25 Formation of SAM's layer ............................................ 41

Figure 26 E-beam resist coating on SPP substrate ............................................ 42

Figure 27 Mercury vapor lamp [47] ............................................ 43

Figure 28 Au and Cr etch ............................................ 44

Figure 29 Encapsulated resist etching ............................................ 45

Figure 30 Anisotropic etch of silicon oxide nanopillar using Au nanoparticle as hard mask ............................................ 47

Figure 31 PlasmaTherm RIE of silicon oxide for 12 minuates ............................................ 47

Figure 32 Anisotropic silicon etch ............................................ 48

Figure 33 Silicon and silicon oxide nanopillar ............................................ 48

Figure 34 SEM images with varied exposure dose (a) 130μC/cm$^2$ (b) 150 μC/cm$^2$ (c) 160 μC/cm$^2$ (d) 170 μC/cm$^2$ (e) 180 μC/cm$^2$ ............................................ 50

Figure 35 Selective placement of 30nm Au on SiO2 ............................................ 52

Figure 36 Varied Ion concentration (Phosphate buffer solution) (a) 0.1mM (b) 0.5mM (c) 1mM (d) 10mM ............................................ 53

Figure 37 Effect of change in pH concentration of phosphate buffered solution (a) pH 7.0, (b) pH 7.25 and (c) pH 7.5 ............................................ 54

Figure 38 Selective template removal with zoom in (a) and zoom out (b) SEM image ............................................ 56

Figure 39 PECVD of silicon oxide nanopillars ............................................ 57

Figure 40 Thermally deposited silicon oxide nanopillars (a) 30nm DNA-functionalized Au nanoparticle (b) 12 min etching ........................................................................ 57
Figure 41 Silicon/silicon oxide nanopillar with $SF_6$ and $CHF_3$ with TRION DRIE for 60seconds ........................................................................................................ 58
Figure 42 Silicon/silicon oxide nanopillar with $CF_4$, He and $O_2$ with TRION DRIE for 60seconds ........................................................................................................ 59
Figure 43 Silicon/silicon oxide nanopillar with SF6 and CHF3 with TRION DRIE for 60seconds ........................................................................................................ 59
Figure 44 Silicon/silicon oxide nanopillar with $SF_6$ and $O_2$ with TRION DRIE for 60seconds ........................................................................................................ 60
Figure 45 Silicon/silicon oxide nanopillar with $CF_4$ with TRION DRIE for 60seconds 60
Figure 46 Helium base flow (a) 5 sccm (b) 4 sccm .................................................... 61
Figure 47 Step height of silicon etch ........................................................................ 62
Figure 48 Silicon nanopillar ...................................................................................... 62

# List of Tables

Table 1 The average values including standard deviations for particle sizes, absolute number of oligonucleotides per particle, surface coverage, effective footprint and calculated deflection angle. ........ 20

Table 2 surface coverage of DNA on gold Nanoparticles from 15 to 250nm at 1.0M NaCl after sonication for all spacers [38] ........ 20

Table 3 Mixtures of phosphate buffered solutions ........ 54

Table 4 Etch of resist ........ 55

# Chapter 1
# Introduction

## *1.1 Motivation and Approach*

Nanopillars have been investigated over the years because of their novel electrical and optical properties that could not be obtained from the bulk materials. Nanopillars have many applications such as fabricating transistors, photo voltaic cells, solar cells and sensors [1] [2] [3]. These structures have high surface to volume silicon ratio, high light absorption efficiency and unique quasi one-dimensional electronic structure. Application of nanopillars in field effect transistors has led to miniaturizing the electronic devices and development of new device concepts like junctionless transistors and new functionalities on the device level [4]. However, fabricating these nanopillar devices and sensors requires controllable placement of nanopillars at precise locations on a large scale. Currently, fabrication of nanopillars at exact substrate positions remains challenging. This thesis has investigated a new approach of forming nanopillars at exact positions, in which placement of nanoparticles at exact locations is carried out using electrostatic funneling technique and using the attached nanoparticles as a hard mask for dry etching to form nanopillars.

## *1.2 Thesis outline*

In this thesis, fabrication of single silicon/silicon oxide nanopillars by the top-down process has been discussed in detailed.

In chapter 2, the basic understanding of experimental setup and introduction is presented. Introduction to dry etching has been presented in this chapter with detailed plasma properties. This chapter mainly deals with the different techniques and methodologies used in the fabrication process.

Chapter 3 includes the protocol for the fabrication of nanopillars which are discussed in detail. Overview of different types of equipment used in the process and different chemical reagents used for the fabrication are mentioned. The processes

explained in this chapter include E-beam lithography, developing, deposition using electron beam evaporator, lift-off, surface modification using SAM's layer, single particle placement of Au nanoparticles, template removal leaving Au nanoparticles by wet etching and formation of silicon nanopillars using dry reactive ion etch as gold as a hard mask.

Chapter 4, results were discussed in detailed using different dosage in E-beam lithography, different pH, and ion concentrations when placing Au nanoparticles and different dry etches chemistries in a reactive ion etch. Scanning electron microscopy is used for interpreting the different chemistries and values in the fabrication process. Usage of wet etch chemicals have been discussed along with etching rates for the formation of template leaving Au nanoparticles on the silicon oxide surface.

Chapter 5, for the above results and discussions conclusions were drawn with the available data. Finally, future prospects have been discussed for any further developments.

# Chapter 2
# Background

The aim of this thesis is to develop an approach for large scale fabrication of silicon nanopillars at exact locations. This chapter gives a brief description of various techniques employed for the fabrication of nanopillars by other researchers, factors effecting the placement of nanoparticles and gives a basic understanding of various experimental steps involved in the fabrication process.

## *2.1 Fabrication of Nanopillars*

### 2.1.1 Nanopillar Fabrication Using Top-Down and Bottom-Up Approaches

Nanopillars exhibit novel electrical properties which has led their use in developing field effect transistors. Nanopillar in FET devices has advantage of forming gate oxide around the nanopillar which has optimum control over the potential. Theodore has fabricated a FET device using silicon nanopillar with a top down approach [2]. Fabrication of these silicon nanopillar in the application of developing FET device is achieved by placing Au nanoparticles on the substrate randomly and anisotropic etching of substrate using Au has hard mask. Layers of gate oxide and gate electrode are evaporated to have active contact between formed vertical FET device which is made from single nanopillar. Nanopillar is etched to form a nanopore which is later deposited with thin oxide and conductive layer on the interior of the nanopore. The top and bottom layer of nanopore forms drain and source region with appropriate doping.

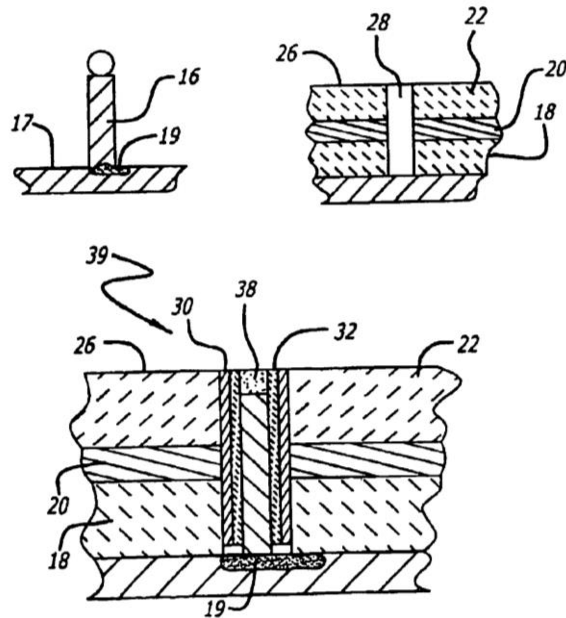


Figure 1 Fabrication of FET device

M. T. Björk and et al. have fabricated a FET device using bottom up approach using vapor solid liquid growth mechanism on the silicon substrate with help of a gold catalyst [1]. FET devices were fabricated in such a way that they have top metal contact and a partially surround-gated channel. Deposition of gold material as a catalyst has been placed by using E-beam lithography which has a low through output during large scale fabrication. The below figure shows the processing of vertical Si nanopillar transistors.

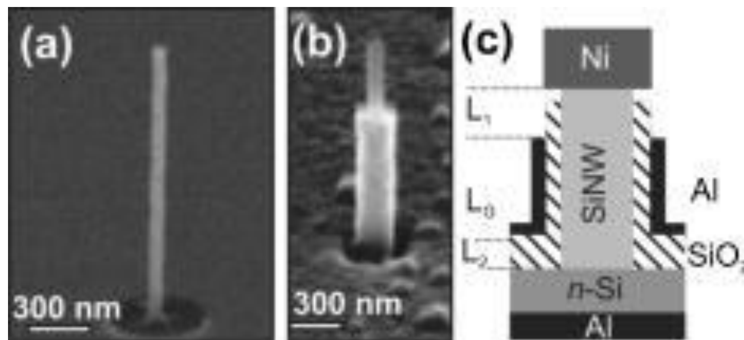


Figure 2 Processing of nanowire silicon transistor

### 2.1.2 Nanopillar Fabrication by Controlled Oxidation

Fabrication of silicon nanostructures can be employed using controlled oxidation method which was employed by Christopher et al. This technique includes development of oxide on the silicon substrate and application of lithography process to transfer patterns on the $SiO_2$ substrate. Resist as a hard mask, $SiO_2$ is etched to form the pattern and later used as a hard mask for deep silicon etch. A series of controlled oxidation and wet etching of oxide layer is carried out for the formation of nanopillar [5]. The below schematics depicts the fabrication steps involved in the development of nanopillar by controlled oxidation.

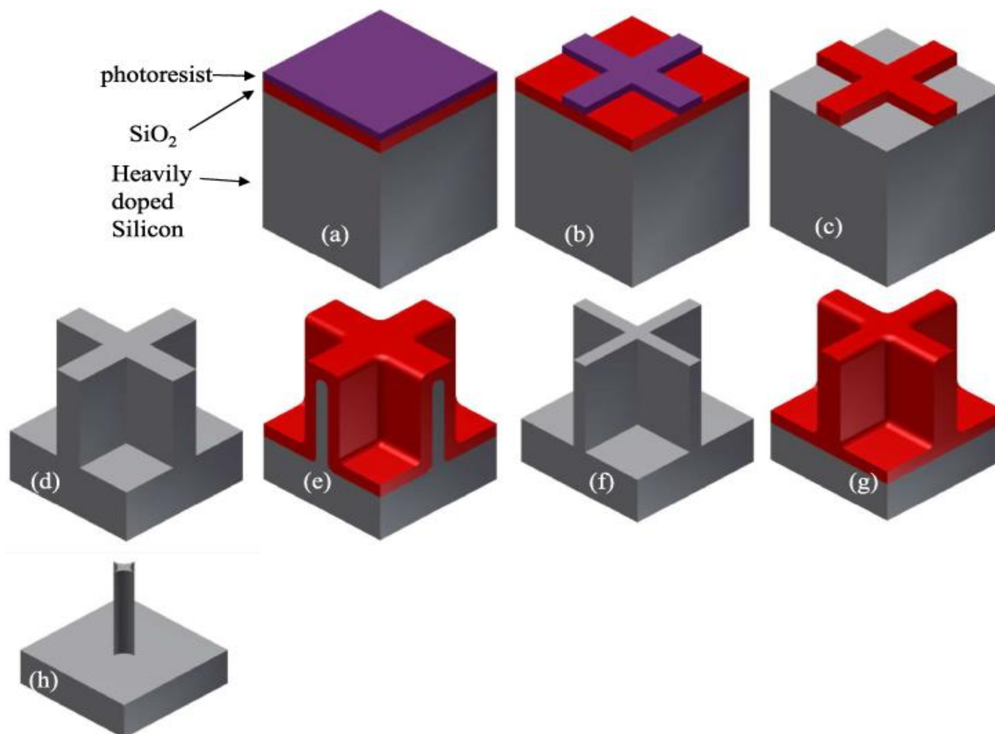


*Figure 3 Schematic depiction of fabrication sequence for silicon nanopillar arrays using controlled oxidation a) Photoresist on thermally oxidized silicon wafer b) Photolithography used for a feature size of 500 nm c) Etching oxide film d) Etching into silicon substrate e) Oxidizing Si f) Stripping oxide g) Oxidizing Si h) Stripping oxide [5]*

*3.2 Fundamentals of charge carriers*

This section deals about the electrostatic interaction between charged Au nanoparticle, silicon oxide and gold substrate. Factors affecting the interactions is also discussed in below sections.

3.2.1 Zeta Potential

The potential difference existing between the surface of a solid particle immersed in a conducting liquid and the bulk of the liquid [6] [7]. The electrostatic potential at the slipping plane is known as zeta potential as shown in the below figure. Zeta potential is generally calculated to know the strength of surface potential.

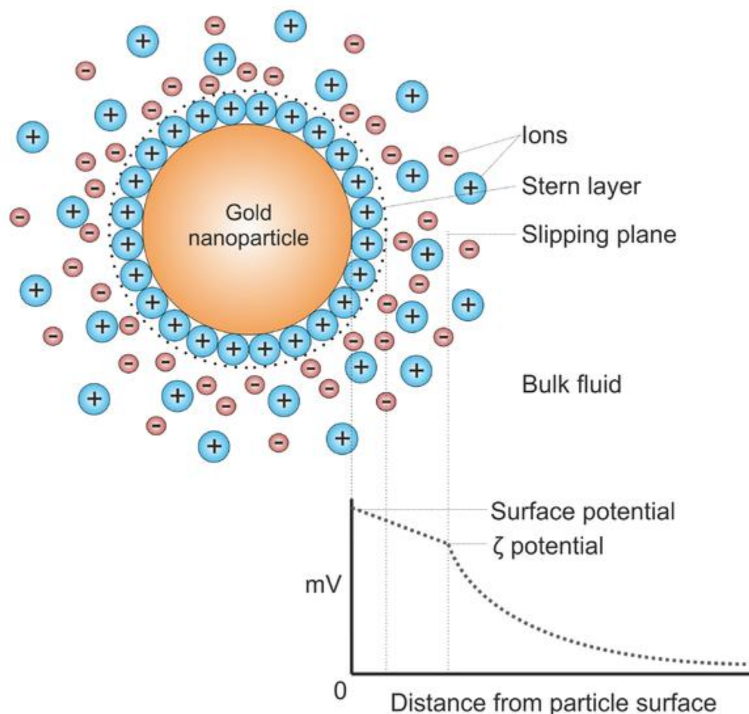


*Figure 4 Schematic representation of ionic charges around a charged particle in a aqueous media*

Aqueous colloidal solutions contain positive and negative charged particles due to the presence of ionic particles in the solution. Negatively charged nanoparticle when introduced in the solution, positive ions present in the solution gets attracted to

the nanoparticle to form a compact layer called stern layer [8]. Ions which are attached to the negatively charged nanoparticle screens halfway. Attachment of additional positive charged particles to the negatively charged nanoparticles, forms another layer called diffusion layer. Formation of these two layers is known as double layer [9] [10]. In diffusive layer ionic concentration is not same as the bulk, there is a gradient on the concentration of ions outward from the particle unit it matches the bulk. When a nanoparticle migrates in the solution, ionic charges that are near to nanoparticle surface move together with nanoparticle, defining a limit called slipping plane. The electrostatic potential at the slipping plane is the zeta potential.

The value of zeta potential estimates the stability of a nanoparticle colloid. Nanoparticles with high zeta potential are steady, since they high repulsive forces between them which prevents agglomeration. Whereas, particles with low potential are not steady and can endure accumulation. Nanoparticle with a higher zeta potential will have more grounded electrostatic associations between the nanoparticles furthermore between the nanoparticle and charged substrate surface.

### 3.2.2 Debye Length

In this thesis carrying out single particle placement is done with various pattern diameters on the silicon oxide substrate. To decide the pattern diameter calculation of Debye lengths are very important [11] [12]. At the point when colloidal particles are scattered in a medium containing free ionic particles, the electrostatic communications will be screened by these ions. The Debye length is the distance over which a charge Q is shielded by the ions in a solution. What this implies, alluding to the photo at the bottom, is that the overabundance ionic charge inside the circle of sweep $\lambda_D$ is around equivalent to charge –Q, in this way counteracting the field of the +Q of the first charge at separations advance than $\lambda_D$. There is overabundance ionic charge in this circle on the grounds that, if Q is sure, negative particles are pulled in into the circle and positive

particles are repulsed from the circle, leaving an overabundance of negative charge in the circle.

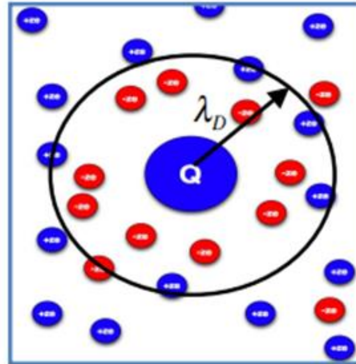


*Figure 5 schematic of Debye length*

Calculation of Debye length can be drawn from

$$k = [(\frac{1000e^2\mathrm{N_A}}{\epsilon\varepsilon_0 KT})\sum_i z_i^2 M_i]^{1/2}$$

Where:

k: Inverse of Debye length

$N_A$: Avogadro's number

$Z_i$: Valence of ion species i

$M_i$: Concentration of ion species i

ϵ: Dielectric constant of water

$\varepsilon_0$: Permittivity of free space

This thesis carried out different salt concentration in the aqueous solution to alter the Debye lengths. Phosphate buffer solution is used during the single particle Au attachment. This PB solution contains [$Na^+$], [$H_2PO_4^-$], [$H^+$] and [$OH^-$]

### 3.2.3 Factors Affecting SPP

Au nanoparticle, substrate of gold and silicon oxide are charged to have electrostatic interaction to have guide the nanoparticle to exact location. Charge

densities on the particles depend on ionic and pH concentration of the solution. Charge of DNA functionalized Au nanoparticle is dependent on the length of the strand immobilized onto the surface and number of DNA strands attached to the surface of nanoparticle. We will discuss in detail the dependences of charge densities and Debye length.

#### 3.2.3.1 DNA

DNA is negatively charged in an aqueous media due to the presence of phosphate bonds, phosphate ionizes by releasing hydrogen ions and makes the DNA negatively charged [13] [14]. The negative charge of DNA can be utilized to control the effective surface charge of nanoparticles by attaching DNA molecules to the nanoparticle surface by increasing the salt concentration during immobilization. Research has demonstrated that molecule surface charge can be increased by increasing number of DNA strands attached to the nanoparticle [15]. Loading of DNA strands to the nanoparticle is attributed to NaCl concentration which is primarily ascribed to screening impact of the concentrated counter-particles on the electrostatic repulsion force between the DNA strands [16] [17]. The below figure shows the number of strands bound to the nanoparticle versus change in NaCl concentration.

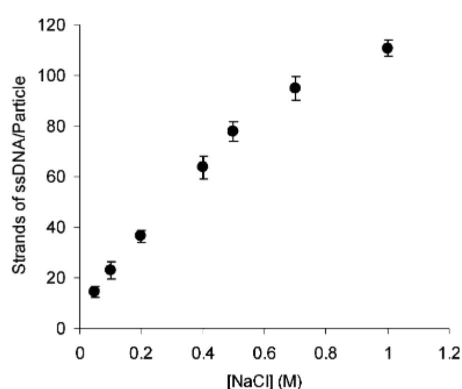


*Figure 6 Surface density of thiol terminated DNA on 13nm gold nanoparticle as a function of NaCl concentration*

Effect of spacer for the DNA strands has also been investigated by the researches for any change in the charge density using Poly-T, Poly-A and PEG spacers. Nucleobase (A) has greater affinity than nucleobase (T) during attachment to the gold surface. Oligonucleotides with Poly-A spacer will probably lie on the gold surface and reduction in the surface thickness. As such, Poly-T spacer attach to the surface perpendicular which has a greater room for attaching more DNA strands to the surface [18].

### *3.3 Experimental Background*

#### 3.3.1 Lithography

Lithography is a microfabrication technique used to make microelectromechanical systems and integrated circuits. Fabrication of these integrated circuits includes a variety of physical and chemical processes to be carried out on substrate namely silicon. Development of these devices requires a various process such as deposition, patterning and etching. Different metallic conductors such as gold, chromium, etc. and insulators namely oxide layer, silicon nitride and others are used to interconnect the circuit or isolate from the components respectively. Creating selective deposition, etching or doping makes the device behave relatively with the applied voltage on the circuit. Underlying theory for all these processes is lithography, transforming the pattern over the substrate making interconnections and isolations so as to form integrated circuits.

Bottom-up process for a basic lithography process includes substrate cleaning, resist coating, exposure, development and pattern transfer. Usual substrate cleaning includes RCA clean for eliminating organics and at times HF or Piranha clean is carried out to make sure the surface is free of oxides and metallic particles on the surface. Cleaning helps in improving adhesion of the photoresist and uniformity over the surface.

The photoresist is a light-sensitive material used in the process of photolithography to form a patterned such that leaving trenches on the surface. The basic function of a photoresist is a change in the solubility of the resist when exposed to light when placed in a developer solution. Some of the general positive photoresist, a photoactive compound which is not soluble in the developer, when exposed to UV light about 350-450nm wavelength is changed to carboxylic acid. The produced end product is easily soluble in the basic solvent. Change in the intensity of the light may have spatial variation in the solubility of the resist in the developer. The photoresist is generally of two types, firstly positive resist, when exposed to a light increase in the solubility of the resist and secondly, negative resist hardens up when exposed to light.

Exposure of light on the substrate is carried out by many means of lithography namely, Optical lithography, UV lithography, Immersion lithography, Electron-Beam lithography namely and such. In this research, I have used E-beam lithography due to its high resolution having patterns of size about 100nm.

#### 3.3.1.1 Electron Beam Lithography

Fabrication of infinitesimal features has been of great needs with recent trends in microfabrication. Devices produced in recent times are getting smaller and smaller, so as to meet those requirements precise patterning techniques must be developed. Many lithography techniques, which use different forms of radiation, include extreme UV, x-ray, electron beams and ion beams to offer high resolution [19]. Out of which electron beam lithography has left some significant role in patterning small devices in their fabrication despite their low throughput in the process. Photolithography techniques has been developed with feature size less than 100nm in the industry with immersion lithography, EUV lithography and so on. E-beam lithography is favored in academia because of unavailability of advance techniques in photo lithography. Examples of nano devices produced with the aid of electron beam lithography have a

wide range of their applicability in calibration, electronic devices and optics components [20].

Electron source has the benefit of extremely high diffraction-limited resolution and has been used for transferring patterns onto silicon substrates with nanometer range [20]. Electron beam lithography takes the advantage of computer-aided design (CAD) for designing the patterns to expose beams on the substrate. These CAD designs replicate the usage of chromium masks used in photolithography in transferring patterns [21]. These CAD designs have aided in altering the patterns easily and quickly.

Electron beam lithography is carried out in two different ways, projection printing and direct writing. In projection printing, a large area of the focused beam is exposed onto a substrate with the mask in between whereas direct writing uses a small spot of electron beam focusing on a resist coated substrate eliminating expensive mask [20]. Direct write systems use small focused round beams that move with the wafer to expose the wafer one pixel at a time. This system consists of a source of electrons, focusing magnetic lenses, blanker to turn beam on and off, deflection system for moving beam and stage for holding the substrate [20].

Electron beam lithography has a greater resolution because of the smaller wavelength of order 10-50 Kev electrons. Usage of these short wavelengths with possible energy densities makes this technique have precise patterns in nm range. The focused electron beam is exposed to the substrate through SEM containing electron sensitive resist on the surface. The advantage of using this technique is eliminating the use of mask and its related difficulties.

### 3.3.2 E-Beam Resist

E-beam resist is a chemical compound which is electron beam-sensitive used mainly in semiconductor fabrication techniques such as E-beam lithography to form a pattern. Resists are normally coated on the substrate to trace the patterns defined in

CAD to be transferred. Resists are high molecular weight polymers dissolved in a liquid solvent. The resist liquid is spin coated on a substrate to form a thin coating. Polymeric structure changes when exposed to a beam of electrons, which makes the film hardened or lessen up depending on the chemical used. Craving properties for good resist are high sensitivity and high resolution. The resist can either be positive or negative resist.

- Positive photoresist, when exposed to light, becomes soft and which is soluble when placed in photoresist developer. The unexposed area of the photoresist is insoluble in the developer. A solvent developer rinses off the weakened resist on the substrate leaving positive tone pattern.
- Negative photoresist, when exposed to light becomes hard and is insoluble in photoresist developer. Unexposed area is soft and is soluble in the developer.

Commonly used light sensitive exposure are Ultraviolet, Deep Ultraviolet and g and I lines having a wavelength of 436nm and 365nm respectively of a mercury-vapor lamp. In this study, I have used electron sensitive resist for the formation of patterns on the substrate. Working principle of the photoresist under light is similar to the electron sensitive resist, source for the formation of patterns is electron beam exposure onto the substrate.

### 3.3.3 SAM's Layer

Development of self-assembly is observed without any external sources other than that are available in nature [22]. Self-Assembled Monolayers (SAM's) are formed at gas-liquid, gas-solid and liquid-solid interfaces [23]. For an ordinary SAM's layer, the sensitive head group forms a molecule-substrate connection of framework [24]. On the different hand, van der Waals forces do act between the molecules including long-range or short-range in order to maintain molecular assembly over the substrate.

Developments in the wide variety surface chemistries on the substrate, their applicability in microanalysis, biotechnology, nanofabrication and corrosion protection has increased [25].

SAM’s are highly ordered organic molecular assemblies that form spontaneously on a variety of surfaces. Formation of SAM’s is created by chemisorption of head groups onto a substrate from state or gas phase with two-dimensional organizations on the substrate. SAM’s are different from surfactant monolayers as they have specific interaction with the substrate of interest [26]. Extensive research of SAM’s layer has been over the past few decades because of its wide usage in applications such as lubrication, corrosion, catalysis and optics to biomedicine and artificial enzymes [27].

These layers help the substrate to act as positive or negative depending on the molecules used. Head groups in SAM’s have high affinity towards the target substrate which is attached by adsorption. Formation of SAM’s layer does not require any high vacuum system or any specialized equipment. There are a number of head groups that have specific binding to a different substrate such as gold, semiconductor, metal oxides and glass [28]. Amine and carboxyl terminated functional groups have been used for silicon oxide and gold substrate so as to from a net positive and negative charge [29].

Thiol molecules are the fundamental building blocks for the formation of SAM’s layer on the metal surface by a bottom-up approach. These thiols can be alkyl disulfides, dialkyl sulfides, alkyl thiosulfates, organic xanthates and alkyl thiocyanates on metal surfaces [25]. Thiols adsorb on the surface forming a thiolate-metal bond at room temperature succeeded by dissociation of S-H bond. Produced hydrogen atom in the above reaction can be eliminated or adsorbed forming a hydrogen molecule. By altering the concentration, doses and time layers can be in lying down or standing up arrangements.

#### 3.3.3.1 Amino-Terminated Functional Group on Silicon Oxide Surface

The coupling agent, 3-aminopropyltriethoxysilane(APTES) used in salinization with silanol terminated silicon is an important surface modification reaction [30]. Formation of APTES on silicon dioxide surface involves two step process. The initial step involves hydroxylation of silicon dioxide substrate and subsequent hydrolysis of APTES ethoxy groups with ethanol as leaving the group, resulting in aminopropyl-terminated surface [30]. Arrangement and density of APTES actively depend on the solvent used in the formation of a monolayer. Hydrolysis of this compound produces ethanol and Tri silanols. Si-C bond in the aminopropyl group will further not cleaved due to its hydrostatically stability. The structure of APTES is shown below.

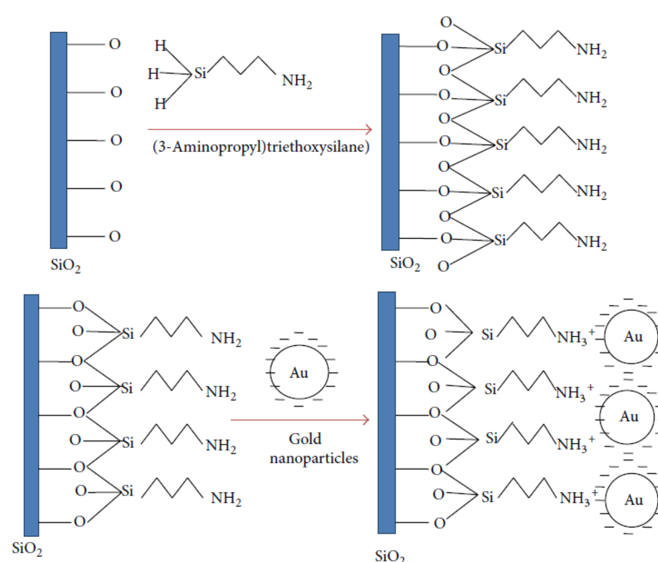


*Figure 7 Surface Modification of SiO2 using APTES [31]*

Formation of APTES on $SiO_2$ surface can be considered in four scenarios during their self-assembly. Particular case one or two ethoxy groups chemically attached to the silicon oxide surface may form cross-linking APTES molecules, which

thus might bring down accessibility for a possibility connection for gold nanoparticles to amine terminal group. In turn time permits situation will be that hydrogen bonds might bond with some of the amine functional groups and -OH from hydroxylated silicon oxide heading $-NH_2$ terminal towards the substrate [32] [33]. When APTES are well adsorbed on the -OH terminated silicon oxide, a full scope of gold nanoparticles on the silanized silicon oxide substrate might a chance to be attained. In this case, every Si bond starting with that APTES molecule might make covalently attached oxygen from the $SiO_2$ surface, resulting in a tripod structure with higher accessible amine groups. These different cases from claiming of APTES formation assume a paramount part in the surface chemistry of the substrate.

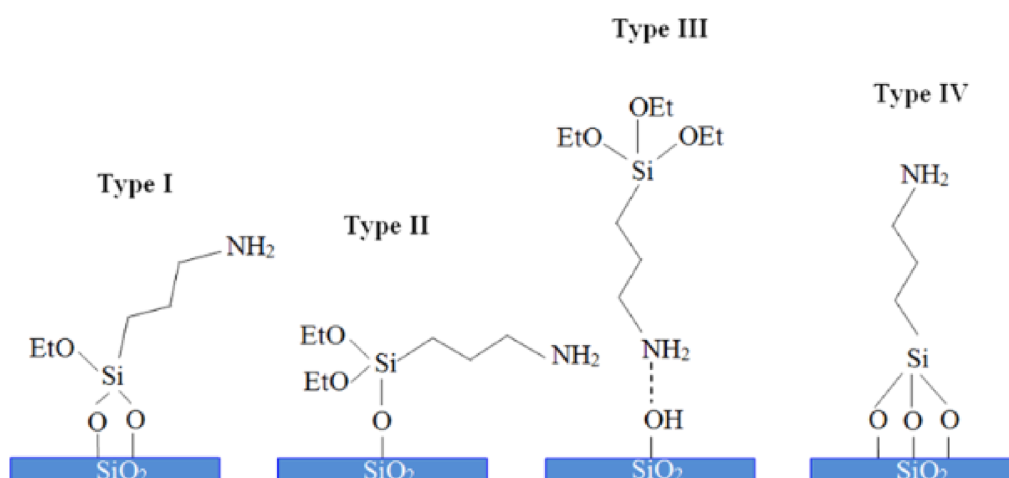


*Figure 8 Schematic representation of possible orientations of APTES molecules on silicon oxide surface [34]*

#### 3.3.3.2 Carboxyl-Terminated Functional group on Gold

Sulfur containing alkanethiols is the common technique for the formation of SAM's layer on gold. Evaporated gold surface on the substrate shows inert behavior for chemisorption of most polar organic functional groups. The contribution of Nuzzo and his coworkers found that disulfide alkanethiol found to be the formation of strong chemisorption bonds [35]. Metallic gold is very compatible in various industries such

as MEMS, bio-engineering and optical engineering. Oxide-free gold surfaces can be easily modified by thiols in liquid phase medium.

Thiols used in the formation of monolayers had three important reasons. First, since gold is an inert material, which doesn’t form oxide surface and any atmospheric contamination. Second, gold has strong specific interaction with Sulphur that allows forming monolayers in presence of many functional groups. Third, these long chain alkanethiols form densely packed monolayers on the gold surface [36].

### 3.3.4 DNA-Functionalized Gold Nanoparticles

#### 3.3.4.1 DNA

DNA (Deoxyribonucleic acid) comprise of two polynucleotides. Every nucleotide is made out of three parts: nucleobase as Adenine (A), Thymine (T), Cytosine (C), or Guanine (G), saccharide sugar or deoxyribose, and a phosphate group. The atomic structure of a nucleotide is shown. Nucleotides are bound together by means of covalent bonds and nucleobases of two polynucleotides are combined together through hydrogen bond in a particular way to such an extent that A dependably matches up with T and C dependably combines up with G.

DNA molecules comprise of two polymer strands which are helical in structure bonded by hydrogen bonds. Processing of single-stranded DNA structure takes place at high temperature and low salt of double stranded DNA.

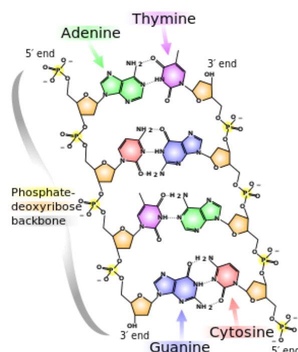


*Figure 9 DNA molecular structure [37]*

#### 3.3.4.2 Functionalizing Au

Mixing of alkanthiol-terminated oligonucleotides with Au nanoparticles, oligonucleotides are immobilized onto gold nanoparticles surface through gold thiol bond. So as will have a thick monolayer about oligonucleotides onto gold nanoparticles surface, NaCl is included of the mixture which shield accuse forces within oligonucleotides. A number of immobilized oligonucleotides onto gold nanoparticle surface relies on salt concentration [38] [39], gold nanoparticle diameter [39] [40] , also Spacer (the length between the distinguish succession and the thiol. adjustment site) creation [41] [42].

##### 3.3.4.2.1 Effect of Salt Concentration

The thickness of the oligonucleotides progresses with NaCl concentration which is principally attributed to the screening impact of the concentrated counter-ions on the electrostatic repulsive force between the surface-bound oligonucleotide strands [38] [39] (Figure below). Hurst et al. Discovered that toward excessive salt concentrations (between 0.7 and 1.0 M NaCl), greatest screening may be attained between neighboring oligonucleotides and stacking remains generally steady [38] (Figure below).

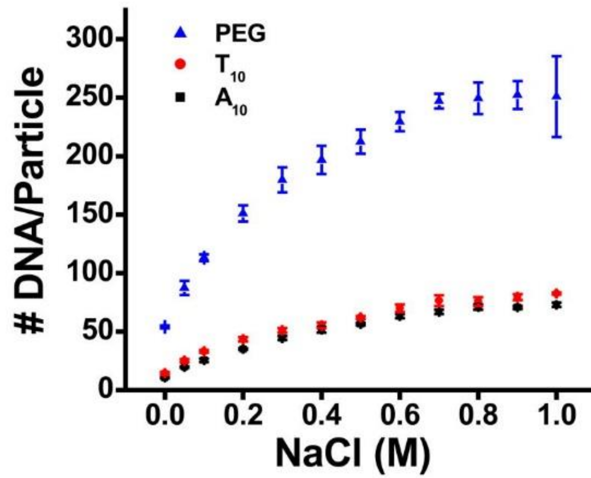


*Figure 10 DNA loading (# DNA strands/nanoparticle) vs NaCl concentration on 15nm Au nanoparticle [38]*

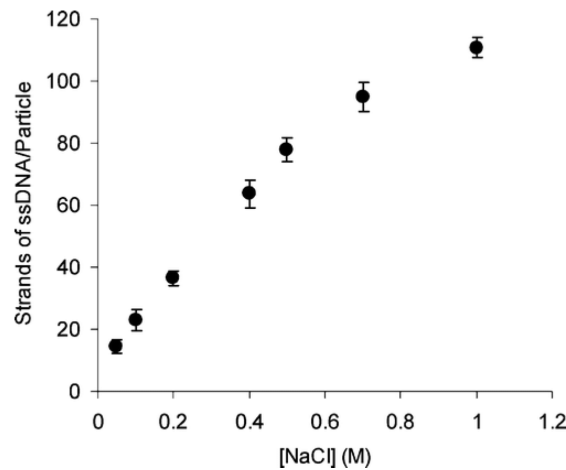


*Figure 11 Surface density of thiolated ssDNA having $T_{10}$ spacer on 13nm gold nanoparticle as a function of NaCl concentration in the immobilization solution [39]*

#### 3.3.4.2.2 Effect of Au Nanoparticle Size on DNA Surface Loading

The impact of gold nanoparticle with respect to surface stacking need likewise been investigated. It need to be been discovered that as the nanoparticle size increases, surface density abatements which will be attributed to diminishing in the curvature of the nanoparticle [38] [40]. Similarly, as a result, DNA strands stand closer

on one another resulting in inter-strand repulsive force increments (Table 1). The impact of gold nanoparticle size on surface thickness may be that's only the tip of the iceberg critical to PEG-containing spacer contrasted with Poly-T or poly-A-containing spacers (Table 2).

*Table 1 The average values including standard deviations for particle sizes, absolute number of oligonucleotides per particle, surface coverage, effective footprint and calculated deflection angle.*

| diameter (nm) | oligos/particle | coverage (oligos/cm$^2$) | footprint (nm$^2$) | deflection (Deg) |
|---|---|---|---|---|
| 10 | 68 ± 10 | 2.0E+13 ± 2E+12 | 4.9 ± 1 | 29 ± 3 |
| 15 | 110 ± 10 | 1.7E+13 ± 2E+12 | 6.0 ± 1 | 21 ± 2 |
| 20 | 180 ± 20 | 1.4E+13 ± 1E+12 | 7.0 ± 1 | 17 ± 2 |
| 30 | 260 ± 10 | 9.3E+12 ± 8E+11 | 11 ± 1 | 14 ± 1 |
| 40 | 430 ± 10 | 8.5E+12 ± 4E+11 | 12 ± 2 | 11 ± 2 |
| 50 | 640 ± 80 | 8.1E+12 ± 3E+11 | 12 ± 1 | 9.0 ± 1 |
| 60 | 890 ± 20 | 7.8E+12 ± 1E+12 | 13 ± 2 | 7.7 ± 1 |
| 80 | 1400 ± 100 | 7.1E+12 ± 9E+11 | 14 ± 2 | 6.1 ± 1 |
| 100 | 2200 ± 200 | 7.1E+12 ± 4E+11 | 14 ± 1 | 4.9 ± 1 |
| 150 | 5100 ± 100 | 7.1E+12 ± 2E+11 | 14 ± 2 | 3.2 ± 1 |
| 200 | 8500 ± 200 | 6.8E+12 ± 1E+12 | 15 ± 2 | 2.5 ± 1 |
| Planar Gold | N/A | 5.8E+12 ± 7E+11 | 18 ± 2 | 0 |

*Table 2 surface coverage of DNA on gold Nanoparticles from 15 to 250nm at 1.0M NaCl after sonication for all spacers [38]*

| Nanoparticle Size (nm) | $A_{10}$ spacer Pmol/cm$^2$ | $T_{10}$ spacer Pmol/cm$^2$ | PEG spacer Pmol/cm$^2$ |
|---|---|---|---|
| 15 | 19 | 38 | 56 |
| 30 | 19 | 35 | 48 |
| 50 | 17 | 19 | 26 |
| 80 | 19 | 20 | 27 |
| 150 | 15 | 18 | 19 |
| 250 | 14 | 16 | 21 |

### 3.3.5 Electrostatic Funneling

Electrostatic Funneling is used in my research for the placement of electrically charged nanoparticle on to certain site-specific location locations which are guided by electrostatic potential energy gradient with nanoscale precision [43]. The substrate is

engineered in such a way that it has a positive and negative charge on the surface when placed in negatively charged gold nanoparticle collide solution, this negatively charged particles are attracted towards the positive surface on the substrate due to electrostatic attraction. Using this concept of electrostatic attraction and by engineering the surface we can achieve placement of nanoparticles at certain locations. Once the nanoparticle attaches to the substrate of the circular pattern area the surface potential mapping of the surface changes such that it prevents attachment of the second nanoparticle onto the surface.

#### 3.3.6 Thermal Oxidation

Silicon (100) wafers were utilized as a substrate for developing silicon oxide nanopillars in the present study. Test evaluation p-type 4" silicon wafers (Nova wafers) were cleaned in acetone ultrasonic bath for minutes to remove the organic impurities on the wafer. The wafers were afterward rinsed with acetone and isopropanol followed by drying with nitrogen. At that point those wafers are drenched in a 10:1 hydrofluoric corrosive bath to 2 minutes should uproot that local oxide formation. Wafer is then rinsed with excessive DI water and blown dry with nitrogen. This step terminates the surface oxide layer for a silicon wafer with the formation layer of hydrogen keeping the structuring from claiming any local oxide layer. The cleaned wafers were after that subjected to Tystar oxidation furnace for developing the wanted thickness of silicon oxide. These wafers were placed in quartz tube held at 450C at a moderate rate of 1 inch/minute which will be preset in the program, to decrease those hazard from claiming thermal shock. Throughout wafer acquaintance under that furnace, those heater tube is continually purged with nitrogen gas with 3 liters/minute. Once the quartz tube totally shuts, those silicon wafers will make in the mid zone of the furnace. The temperature of the heater is gradually ramped to 700C so as to perform oxidation. The oxidation which is performed is a dry oxidation, oxygen I passed through the container for the formation of the oxide layer. Process time for developing the oxide is about one

hour 35 minutes for a height of 150nm. The temperature of the furnace throughout different steps for oxidation process id pre-determined in the Tystar oxidation furnace. The Tystar oxidation furnace is completely automatic once the process parameters are predefined. Once the process is completed nitrogen flow is continued in the furnace tube. The furnace will be cooled down gradually to 700C before opening those wafers. Then wafers were given time to cool before for further any measurements. The thickness of the silicon oxide film developed is checked with Gaertner ellipsometer and Ocean optics NC-UV-VIS reflectometer. Oxygen molecules diffuse easily for the forming oxide layer of $SiO_2$ at high temperatures. Oxygen arriving at the silicon surface can then combine with silicon to form silicon dioxide. The chemical reactions that take place as follow

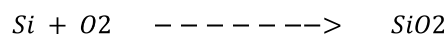

$$Si + O2 \quad -------> \quad SiO2$$

### 3.3.7 Wet Etching

Development of template with gold nanoparticles protected with a resist over it is achieved by wet etching of gold and chromium on the silicon oxide surface. Gold nanoparticles which are exactly placed at the center of silicon oxide surface are protected with resist coating on the surface. Resist etching was done to the height of the gold surface such that deposited gold surface is exposed. The sample is subjected to wet etching of gold in a gold etchant for 5 seconds. The gold etchant is a composition of potassium iodide and iodine, which has an etch rate of 28 angstroms per second. Chrome etching is followed by gold etching to strip off the chromium layer on the silicon oxide surface. Chrome etchant is a composition of perchloric acid ($HClO_4$) and ceric ammonium nitrate $(NH_4)_2[Ce(NO_3)_6]$. Chrome etchant has an etch rate of 40 angstroms per second.

### 3.3.8 Dry Etching

#### 3.3.8.1 What is Plasma?

Plasma is a hot ionized gas consisting of an equal number of negatively charged electrons and positively charged ions. Plasma is considered to be the fourth state of matter since they are significant from neutral gasses. Plasma is strongly influenced by electric and magnetic field while neutral gasses are not. The plasma density is referred to as electron density and ion density which are equal to one another. Plasma is a conductive interface when a radio frequency power is applied between two anodic and cathodic electrodes, electrons are accelerated by the applied power which in turn acquire kinetic energy and collide with atoms and molecules. If the acquired kinetic energy is greater than ionization energy, an electron from the outermost shell is forced to leave. The ejected electron in the electric field media accelerates along with the previous electron collided to form many ions in the chamber. An electron from a neutral atom which is forced to leave results in the formation ion in the chamber. Progressing with the above reactions leads to having an equal number of ions and electrons in the chamber. Increasing in the number of electrons and ions in the chamber reaches a threshold level which results in discharge and creates plasma.

This section deals with the introduction of plasma since dry etching process requires plasma for anisotropic etching. Plasma refers to an ionized gas which consists of an almost equal number of electrons and ions having net neutrality in nature. RF power applied to a pair of electrodes in etching chamber, electrons are accelerated by an electric field generated by RF power, where plasma is conductive in nature, acquire kinetic energy and collide with atoms and molecules. When an electron hits the atoms with high energy, an electron from the outermost shell gets expelled and results in formation of the ion. These number of collisions in the chamber increases eventually reaching the threshold level over which resulting discharge begins and creates a

plasma. Generation of this plasma in the chamber is favored by inducing certain gas such as $O_2$, $CF_4$, $SF_6$, so on. The schematic of dry etching is shown below [44].

- Reaction species are generated in the plasma.
- Species are transported and adsorbed on film.
- Reaction takes place on target film and by-products are formed.
- Byproducts are desorbed.

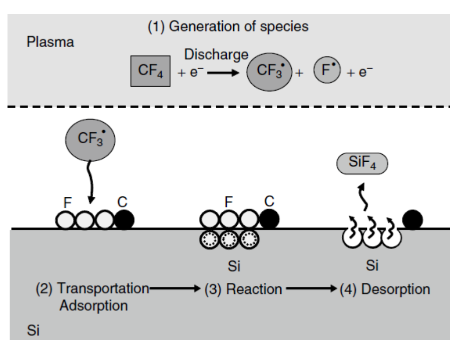


*Figure 12 Mechanism of dry etching [45]*

#### 3.3.8.2 Plasma-Them RIE

Plasma-Therm reactive ion etcher has been used for ashing the resist to make sure the Au nanoparticles are protected during wet etching and development of silicon oxide pillars after the formation of a template having Au nanoparticles at certain pre-defined positions. Thus equipment showed promising results than the Trion DRIE equipment and moreover metal hard masks can be used in this system. This tool was a PECVD deposition tool which has been later modified to RIE. RF power is connected to the top electrode with water cooling pump infused. The bottom electrode is grounded and a heater option for heating samples. The samples were placed on the cathode surface i.e. top electrode for having a higher etch rate and physical etching due to ion bombardment.

100nm thick E-beam resist is spin coated on the sample and placed on the top electrode for the ashing process. The recipe used for the ashing process is 100 SCCM of oxygen at 300mTorr pressure. The power used for ashing is 50 Watt. The ashing

step has an etch rate of 12nm/minute. Then the sample is subjected to wet etching to form template.

Using Au as hard mask silicon oxide nanopillars were formed in the Plasma-therm reactive ion etcher. Thus recipe only consists of $CF_4$ chemistry with a flow of 50 SCCM at 80mTorr pressure. Power used for this process is 200 Watt. Etch was found to be about 10nm/minute.

#### 3.3.8.3 Trion Reactive-Ion-Etching

Trion reactive ion etcher has an ICP unit connected to the top electrode which makes the etch rate to be faster than the normal RIE equipment. This system cannot be used for a metal hard mask because due to its contamination in the inside chamber walls. Several experiments were conducted to determine the right etching condition for silicon/silicon oxide nanopillars.

| Sample Numbers | Gasses | Pressure (mTorr) | Power (W) |
|---|---|---|---|
| Sample 1 | 14 sccm of $SF_6$<br>35 sccm of $CHF_3$ | 10 | 100 |
| Sample 2 | 35 sccm of $CF_4$<br>3 sccm of $O_2$ | 75 | 200 |
| Sample 3 | 15 sccm of $SF_6$<br>50 sccm of $CHF_3$ | 10 | 200 |
| Sample 4 | 30 sccm of $SF_6$<br>16 sccm of $O_2$ | 50 | 100 |
| Sample 5 | 50 sccm of $CF_4$ | 25 | 50<br>And<br>3000W (ICP) |

Out of the following different etch recipes which are taken from literature gas chemistries of CF4 and O2 were best suited for the formation of silicon nanopillars. The

main parameters which really define the etch process depend on electrostatic chuck cooling, temperature, carrier wafer apart from the process parameters. All these experiments were carried after chamber cleaning with oxygen for 30 minutes and a conditioning step for tuning the machine to current recipe.

# Chapter 3
# Fabrication Process

## *3.1 Prototype*

Fabrication of single particle placement device includes thermal deposition, lithography techniques and evaporation of metals on the substrate pattern. Oxide layer is thermally deposited on a silicon substrate with a height of 160nm. Negative e- beam resist is spin coated on the thermally deposited silicon oxide layer for further exposure to electron beam. Exposed resist substrate is immersed in a developer ma-D525 solution to remove the unexposed resist on the surface. Chromium and gold of 50nm and 10nm are evaporated respectively on the resist pattern. Lift-off process is carried out to eliminate the resist pattern having bottom silicon oxide layer exposed. Cleaning of pattern is carried out to remove the scum of negative photoresist on the silicon oxide layer. Cleaning process is carried out in acetone sonication bath for any physical residue on the substrate. Sample is placed under UV/ozone to decompose the organic molecules present on the substrate and modify the molecular surface for assisting the formation of SAM's layer.

- Step 1: Cleaning silicon substrate with acetone, methanol, DI water and dehydrating on a hot plate.
- Step 2: Spin coat of negative e-beam resist.
- Step 3: Exposure of spin coated negative resist to electron beam.
- Step 4: Immersion in development solution.
- Step 5: Evaporation of chrome and gold.
- Step 6: Lift-off process.
- Step 7: Cleaning the sample with acetone sonication bath and exposure to UV/ozone.

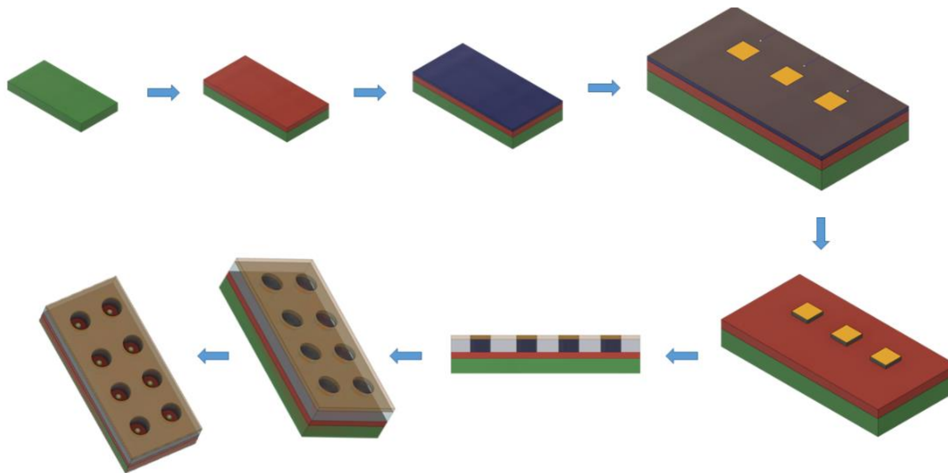

*Figure 13 Steps involved in the fabrication of device*

## 3.2 Experimental Materials

### 3.2.1 Reagents

- Si wafer, p-type (100) (Nova Electronic Materials)
- Ethanol, 200proof ($C_2H_5OH$)
- Acetone ($C_3H_6O$)
- E-Beam photoresist ma-N 2401 (Microchem)
- Photoresist developer ma-D 525 (Microchem)
- 30nm Gold colloid, Tannic coated (Nanocomposix)
- Zonyl FSN-100 (Sigma-Aldrich)
- Synthetic oligonucleotide probe-DNA with disulfide linker (BioBasic)
- DL-Dithiothreitol (Sigma-Aldrich)
- NAP-5 column (GE Healthcare)
- Sodium Chloride, >99.5% (Sigma-Aldrich)
- Sodium Hydroxide (Sigma-Aldrich)
- Tris-EDTA buffer solution, (Sigma-Aldrich)
- 3-Aminopropyltriethoxysilane, 99%, (Sigma-Aldrich)

- Sodium phosphate monobasic monohydrate, ≥ 98% (Sigma-Aldrich)
- Sodium phosphate dibasic heptahydrate, ≥ 98% (Sigma-Aldrich)
- 16-Mercaptohexadecanoic acid, 90% (Sigma-Aldrich)
- Hydrochloric acid (Sigma-Aldrich)
- Chrome etchant
- Gold etchant

#### 3.2.2 Stock Solutions

- **Disulfide cleavage buffer:** 200mM phosphate buffer (pH=8.0)
- **Exchange buffer:** 10mM phosphate buffer (pH=7.5)
- **Salting buffer:** 10x phosphate buffered saline + 3.46 M NaCl (pH=7.5)
- **Storage Buffer:** Tris-EDTA buffer

### *3.3 Experimental Instruments*

- ZEISS Supra 55 VP Scanning Electron Microscope
- ZEISS 1540XB CrossBeam E-Beam Writer
- E-beam evaporator, AJA International
- Oxidation Furnace, Tystar
- Centrifuge, Eppendorf 5418
- Cole-Parmer HP30A Photolithography Hot Plate
- UV- Cure
- Gaertner stokes ellipsometer
- Ocean optics reflectometer
- KLA P6 profilometer
- Plasma Etcher, Plasma-Therm
- Trion ethcher

- Ultra-sonication bath
- Uv-Ozone cleaner
- Millipore DI water purification system
- Spin coater

### *3.4 Substrate Preparation*

The main aim of this section is to make a 100nm circular guided pattern with silicon oxide at the bottom trench and gold on the surface. The whole substrate preparation is done under class 100 clean room fabrication techniques. For a defect free pattern substrate wafer, cleaning and sample handling techniques are crucial in fabrication. One should be careful with handling the e-beam resist as it is very sensitive to moisture. The below figure shows the size of the prepared sample and the patterns developed after gold deposition.

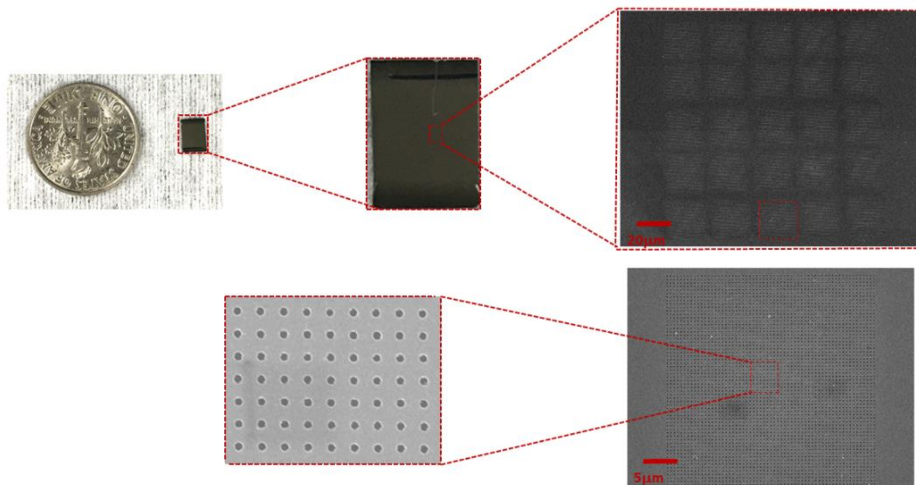


*Figure 14 Sample size*

#### 3.4.1 Si Wafer Cleaning

- Si wafer (4” dia.), p-type (100) is placed in acetone solution in a ultrasonication bath for about 10 minutes and then rinsed with methanol and running DI water. Dry with $N_2$. This is done to remove the organic contamination on the surface of the silicon wafer.

- The above-processed silicon wafer is then subjected to immersion in a piranha solution. Piranha solution is made of 3 parts of 98% sulfuric acid and 1 part of 30% hydrogen peroxide. This solution must be freshly prepared as the stock solution do not have that ability to remove a thin oxide film on the surface of the silicon when exposed to the atmosphere.

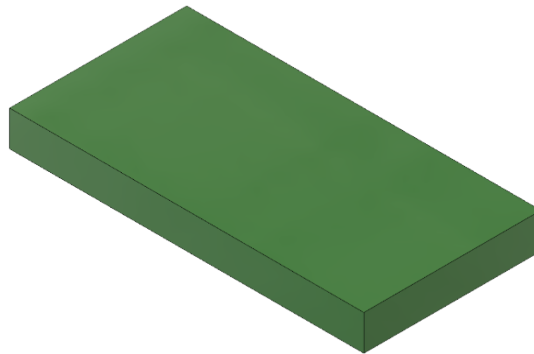

*Figure 15 Bare silicon wafer*

### 3.4.2 Thermally Deposited $SiO_2$

- Cleaned Si wafer is then subjected to dry oxidation in Tystar Furnace.
- Dry oxidation of silicon wafer is carried out at 700C for 95 minutes giving oxide deposition of 160nm over the silicon surface.

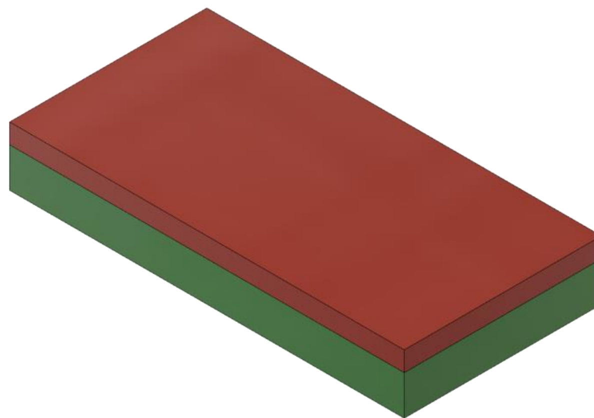

*Figure 16 Thermally deposited silicon oxide*

### 3.4.2 Sample Cleaning

- Grown 150nm dry $SiO_2$ layer is cleaned for further process of spin coat of E-Beam resist.
- $SiO_2$ sample is cut into a small wafer of size 1cm x 1cm with the help of diamond tip indenter.
- Small silicon wafer is cleaned in acetone using ultra-sonicator at room temperature for 10 minutes. Rinsing with methanol and running DI water thoroughly.
- Dry with $N_2$.

### 3.4.3 Spin Coat Negative E-beam Photoresist

- Before spin coating, sample should be dehydrated at 200 $^0$C for 20 minutes.
- Spin coat the negative e-beam resist ma-N 2401on to $SiO_2$ wafer piece with a two-step process.

  Step 1: 500rpm for 5 sec

  Step 2: 3000rpm for 30 sec
- Step 1 is used for spreading the resist onto the surface of the $SiO_2$ wafer and the successive step is preferred for thinning of the resist to about 100nm.
- Pre-bake the small wafer at 90 $^o$C for 1 minute.
- Three indentation marks were marked on a single 1cm x 1cm sample for reference to expose the patterns just below the marks.

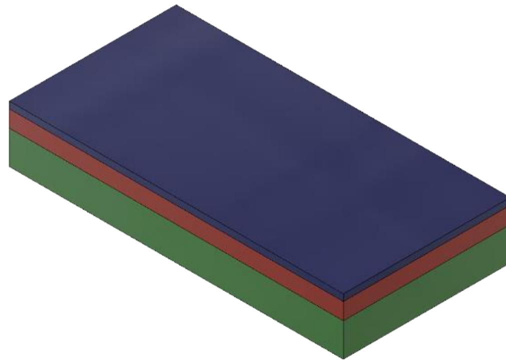

*Figure 17 E-beam resit coating on silicon oxide*

#### 3.4.4 E-Beam Lithography

- Spin coated wafer is then exposed to e-beam (resist sensitive to e-beam) to form certain patterns on the surface which are predefined in the NPGS software on the E-beam writer.
- Circular guided patterns are first developed in AutoCAD package and then transferred to NPGS software in the e-beam writer computer.
- E-beam exposure dose is set to 150 $\mu C/cm^2$.
- 30kV with 10nm aperture is used for writing.
- Line to line and center to center spacing of beam exposure is optimized for defect-free patterns with minimal change in assigned dimensions.

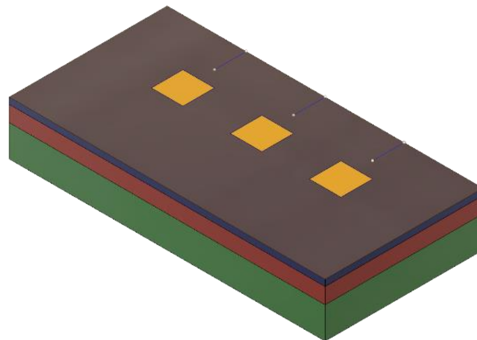

*Figure 18 E-beam exposed patterns on negative resist*

### 3.4.5 Development

- Exposed e-beam pattern has patterns with an area with soluble and insoluble to photoresist developer.
- Ma-D 525 developer is used for 10 seconds to remove the soluble resist and form cylindrical resist blocks on the substrate.
- Substrate is then transferred to Di water bowl to wash for about 5 minutes such that to remove the residue on the substrate. Dry with $N_2$ gently as it may affect the cylindrical resist on the surface.

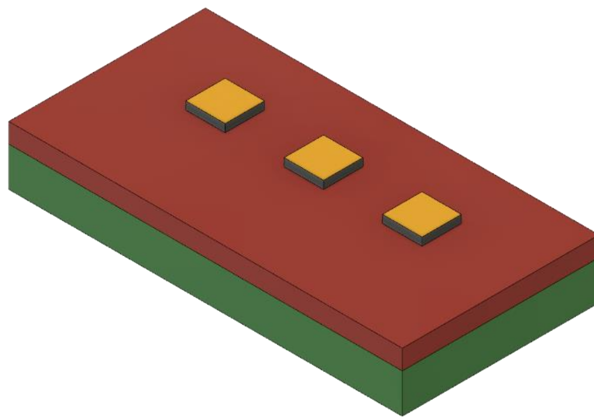

*Figure 19 Developed resist patterns*

### 3.4.6 Evaporation

- Evaporation of Cr and Au is done with AJA International.
- This evaporation is evaporated under high vacuum.
- Deposition of Cr is usually evaporated to form a good adhesion between the substrate and gold. 50nm of Cr is evaporated on the substrate with resist patterns on it.
- Later on, 10nm Au is evaporated on to the wafer piece.

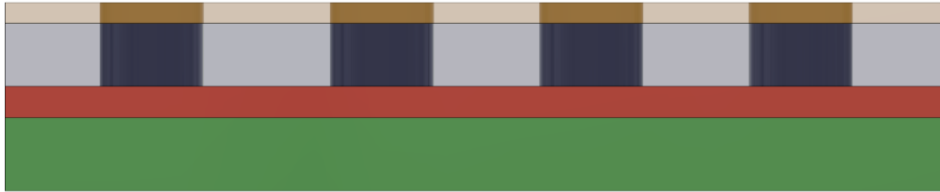

*Figure 20 Chrome (50nm) and gold (10nm) deposition*

#### 3.4.7 Lift-off and Cleaning

- A lift-off process is usually done with acetone in the ultra-solicitor bath for about 30minutes.
- Finally, we have fabricated our device with $SiO_2$ trench and gold surface with circular patterns of about 100nm.
- Cleaning the gold-coated $SiO_2$ wafer piece by acetone and UV-ozone cleaner at room temperature for 10 and 10min. This step is repeated 5 times to make sure the sample is clean for further action.
- Cleaned sample is then placed in ethanol overnight to break the gold oxide formed.

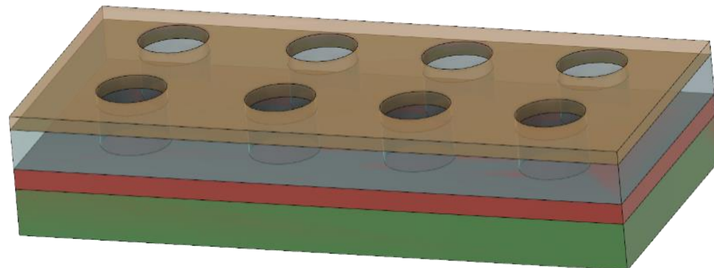

*Figure 21 Lift-off process*

### *3.5 Single Particle placement*

This section mainly deals with the placement of gold nanoparticle on to certain site-specific location of the fabricated device above. Development of DNA-gold

conjugate is used for having a net negative charge on the surface of the gold nanoparticle (GNP). This charged GNP when placed in an ionic and in controlled pH solution has a repulsive and attractive forces acting on the surface of the substrate. Since with the application of SAM's layer on the surface of the substrate having a positive charge on $SiO_2$ surface due to amine terminated at the end and negative charge on gold surfaces due to carboxyl group termination end.

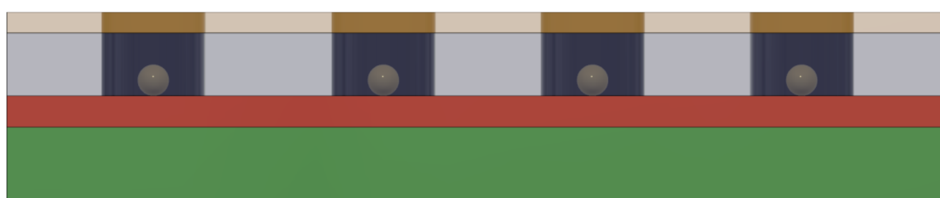

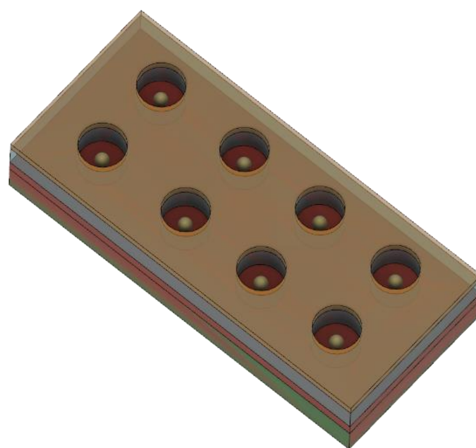

*Figure 22 Single particle placement*

### 3.5.1 Au Conjugate

Attachment of DNA strands on the surface of the gold nanoparticles depends on salt concentration, pH and ionic concentration in the solution during conjugation. Below we will discuss about the preparation of gold nanoparticle conjugate.

- Centrifuge 14.8nmol probe-DNA for 3min at 3000rpm. This is usually done to make sure all the DNA powder is all set the bottom of the tube. Probe DNA is stored in the freezer.

- Prepare 1ml of 0.1M DTT in disulfide cleavage buffer. Add about 125 μl of the above-prepared solution in P-DNA tube, wrap the tube in aluminum foil and shake it for 3 hours on a rotating shaker. DTT is used for the reduction of disulfide bond in the oligonucleotides which later favors the immobilization of DNA on GNP. Cleavage reaction is shown below.

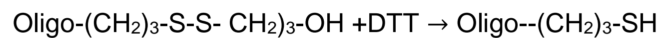

$$\text{Oligo-}(CH_2)_3\text{-S-S- }CH_2)_3\text{-OH +DTT} \rightarrow \text{Oligo--}(CH_2)_3\text{-SH}$$

- Cleaved DNA are further processed through gel filtration using NAP-5 column. This process helps in purification of oligonucleotides on the basis of their size. The column consists of porous matrix structure inside the column which allows small sized oligonucleotides to pass through the gel bed and eliminate larger size oligonucleotides.
    - Nap-5 column is first equilibrated with 15 ml of exchange buffer which allows the buffer to flow through gel bed by gravity flow.
    - Add 125 μl P-DNA cleaved solution into the column and allowing it to enter the gel bed completely.
    - Add 375 μl of exchange buffer into the NAP-5 column and allow entering gel bed completely.
    - Addition of 500 μl of exchange buffer into column and collecting 500 μl of purified DNA at the bottom by gravity flow.
    - NAP-5 column illustrations are shown below

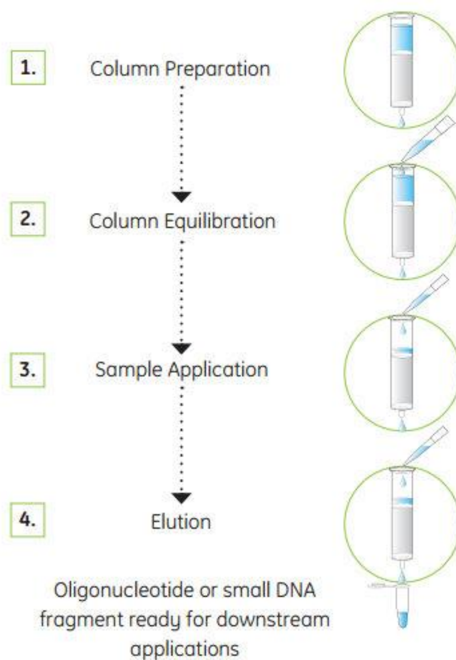


*Figure 23 Working schematics of NAP 5 column [46]*

- Just before the elution process, 950 μl 30nm GNP is transferred to a centrifuge tube.
- Prepare 1ml of 1wt% Zonyl FSN-100 (surfactant) in DI water. This surfactant helps in not forming agglomerates of GNP in the solution at high salt concentrations. Addition of 50 μl of 1wt% Zonyl FSN-100 to 950 μl 30nm GNP and then placed in rotating shaker for 15minutes.
- Add 125 μl purified DNA to GNP solution.
- Addition of 111 μl of salting buffer to GNP to obtain a final concentration of 0.45M NaCl. Vortex the GNP solution, wrap in an aluminum foil and place in rotating shaker overnight.
    - Concentration of NaCl
        - **Salting buffer:** 10x phosphate buffered saline (contains 1.47M NaCl) + 3.63M NaCl
        - **Calculation:**

$$\frac{5 * 111(salting\ buffer)}{950(GNP) + 50\ (Zonyl\ FSN - 100) + 125\ (P - DNA) + 111(Salting\ Buffer)} = 0.45M$$

- Buffer Strength
  - **Calculation:**

$$\frac{(125 * 10)\ (DNA\ in\ Excahnge\ Buffer) + (111 * 100)(Salting\ Buffer)}{950(GNP) + 50\ (Zonyl\ FSN - 100) + 125\ (P - DNA) + 111(Salting\ Buffer)} = 10mM$$

- Centrifuge the DNA GNP for 10minutes at 10,000rpm. Remove the float solution which remains DNA GNP at the bottom of the tube. Suspend this DNA-GNP in 1000 µl of conjugate washing buffer. This centrifuge step is repeated 4 times to make sure the free DNA is eliminated and only DNA functionalized GNP are present in the solution.
- DNA functionalized GNP are then placed in Tris-EDTA buffer solution in its last step. This solution helps in storage the DNA-functionalized GNP for a longer time. This purified DNA is placed in freezer and can use whenever needed.

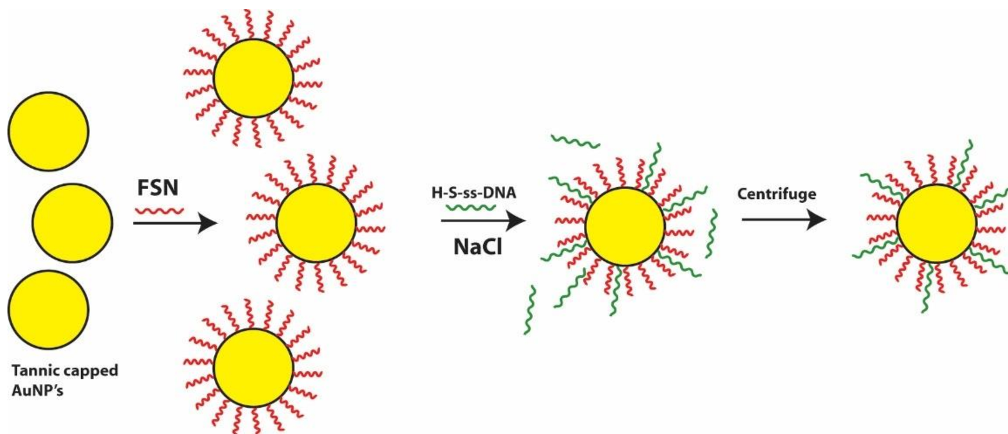


*Figure 24 DNA functionalized Au nanoparticle*

#### 3.5.2 Formation of SAM's Layer

Advancement in the formation of SAM's layer on the substrate helps in guiding the DNA-functionalized GNP onto the silicon oxide surface. Development of SAM's layer is favored by using APTES and MHA, formation of positive charge on silicon oxide by APTES and negative charge on Au surface by MHA respectively.

#### 3.5.2.1 Formation of Positive Charge

3-Aminopropyltriethoxysilae (APTES) is used for formation of positive SAM's layer on the silicon oxide substrate. APTES is prepared in ethanol solution rather than in DI water since it gets hydrolyzed. Ionic strength and pH of the solution are maintained so as to get a uniform self-assembled monolayer on the surface. Procedure for SAM's formation is discussed below

- Device placed in ethanol overnight is rinsed in new ethanol solution and is vortexed for 10 seconds.
- Prepare 0.1 vol% (0.5 ml) of APTES in 500 ml ethanol solution. Vortex for 10 seconds.
- Prepare 0.1M NaOH solution in ethanol and vortex it. Add 0.4 vol% (2 μl) of NaOH in APTES solution.
  - pH of APTES is 10.6
    - NaOH is a strong base (dissociates)
    - $P^{OH} = -\log_{10}(0.0004) = 3.4 \Rightarrow p^{H} = 14-3.4 = 10.6$
- Immerse the device in the above prepared solution for 40 minutes.
- Rinse the device in new ethanol for two times in the same tube and rinse one more time a new tube of ethanol.
- Transfer directly into MHA prepared solution.

#### 3.5.2.2 Formation of Negative charge

16-mercapthohexadeconic acid (MHA) is the chemical compound used for the formation of net negative charge on the Au surface. Preparation of this solution takes place in an acid medium so as to form $COO^-$ terminated on the surface.

- Prepare 5mM of MHA in 500 ml ethanol.
- Add 1 vol% of HCl to MHA solution so as to make the solution acidic.
- Immerse the device into MHA solution for two and half hours.

- Rinse the sample with ethanol two times in the same tube and one more time in new ethanol tube.
- Rinse with DI water squeeze bottle and gently dry with $N_2$.

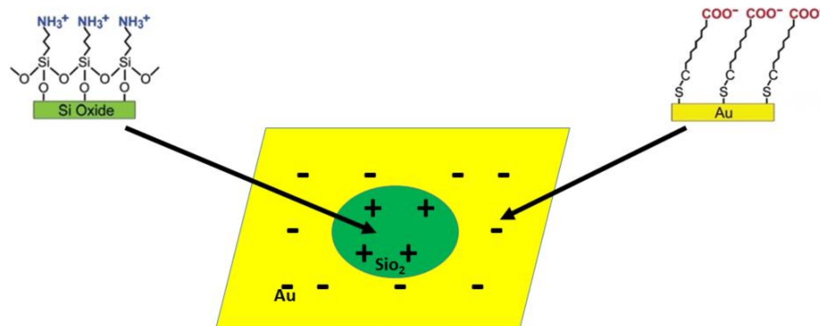


*Figure 25 Formation of SAM's layer*

### 3.5.3 Directed Self-Assisted Au Placement

Directed self-assisted Au placement depends on ionic strength and pH of the solution. 200 μl of DNA functionalized GNP is centrifuged and then suspended into 1mM phosphate buffer solution with pH 7.25. Dried SAM's formation layered substrate is placed in the hybridization chamber and 6 μl of 1mM PB solution pH 7.25 DNA functionalized GNP is placed on the substrate for 3 hours. As the net negative charge of the GNP in the solution attracts towards the positive charged SAM's layer on the silicon oxide substrate and repels on the Au substrate since its negatively charged by carboxyl terminated group on the surface. The schematics of GNP is shown below.

## *3.6 Selective Template Removal*

In this section, we fabricate Silicon oxide template with placed GNP at certain site-specific locations. We strip Cr and Au on the substrate using chrome and gold etchant. GNP is protected using resist spin coat in the trenches of silicon oxide on the device when placed in the gold etchant. Resist etching is carried out with oxygen plasma which is discussed in later sections.

### 3.6.1 Resist Coating

Single particle placement of DNA functionalized GNP is carried out till previous sections. Resist coating allows the GNP to be protected when placed in Au etchant. Ma-N 2401 e-beam resist is used for encapsulating the GNP. Resist is spin coated all over the device and then subjected to plasma-therm oxygen etching such that resist only blocks the trenches and leaves free over the gold surface.

- Ma-N 2401 is spin coated in two steps.
  - First step: 500rpm for 5 seconds
  - Second step: 3000rpm for 30 seconds
- The device is pre-baked at 90 $^{o}$C for 1 minute.

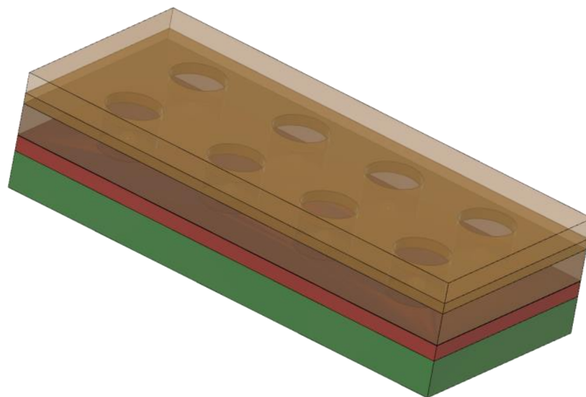

*Figure 26 E-beam resist coating on SPP substrate*

### 3.6.2 UV Curing Flood Lamp

UV curing is carried out to hardened the resist over the device surface which helps in controlling the oxygen plasma etch. The whole sample is exposed to Uv light for about 2minutes at room temperature. When this resist is exposed to the UV light get polymerized forming interlocking of polymers which in turn hardens the resist. This UV lamp is operated with 600 W power to make sure it polymerizes e-beam resist.

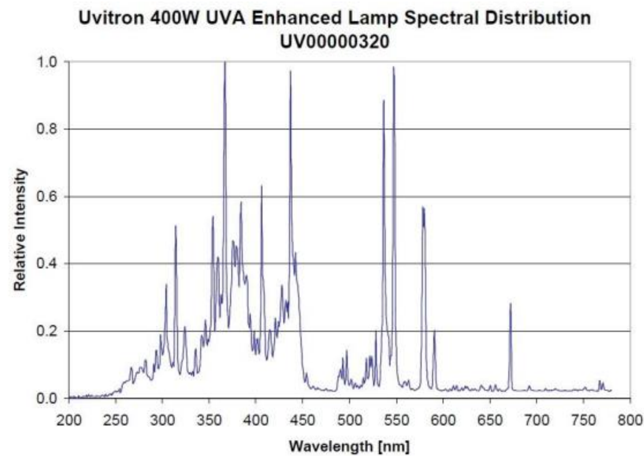


*Figure 27 Mercury vapor lamp [47]*

#### 3.6.3 Resist Strip

Photoresist ashing is carried out in plasma-therm etcher with oxygen gas as gas medium. Ashing of photoresist is carried out in a controllable manner such as way that Au surface is exposed and the circular trenches are filled with photoresist. GNP are encapsulated in these photoresist trenches which is protected from further wet etch of gold. Parameter used for ashing e-beam resist is

- Power: 50W
- Pressure: 300mTorr
- $O_2$ flow: 100 SCCM
- Time: 7minutes

The above parameters are carried out and the etch rate was found to be 120A° per minute. Resist coated on the device substrate was found to 1000A°.

#### 3.6.4 Au and Cr Etch

Device is then subjected to wet etching so as to remove the thin films which were evaporated during lithography. Device is placed in Au etchant for 5 seconds to strip all Au surface on the device. As per the company manufactures specification the etch rate was 28A°/sec. Over etch was carried out to make sure all the gold is etched.

After Au etch the device is rinsed in Di water for 2 minutes to make sure all the Au etched surface is free from small flakes. Device is placed in Cr etchant for 20 seconds to etch all Cr surface on the substrate. Etch rate of Cr is 40A°/sec. Over etch is carried to ensure thin Cr film is etched as it does not affect silicon oxide substrate below.

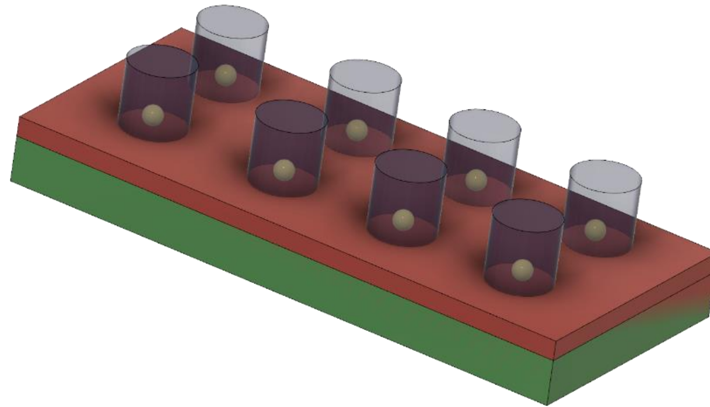

*Figure 28 Au and Cr etch*

### 3.6.5 Cylindrical Resist Etch

We have the device with GNP encapsulated in cylindrical e-beam resist on the substrate. We carry out oxygen plasma etch remove the e-beam resist, which makes the GNP exposed on the surface of silicon oxide surface. Parameter used for ashing e-beam resist is

- Power: 50W
- Pressure: 300mTorr
- $O_2$ flow: 100 SCCM
- Time: 10 minutes

Over etching is carried out to make sure all the resist scum on the surface is clean.

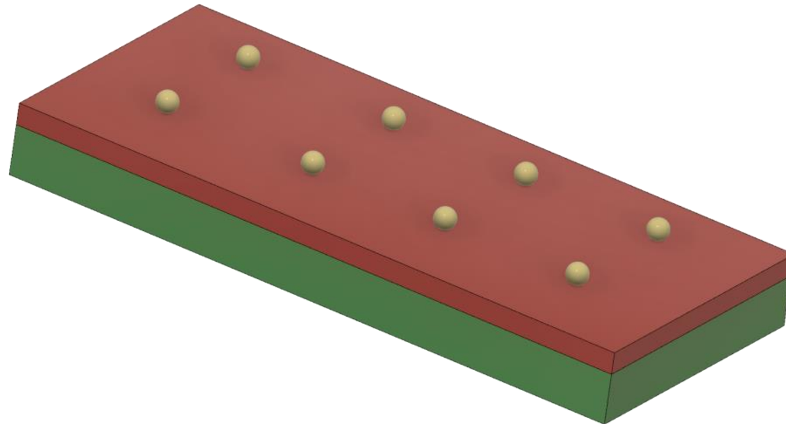

*Figure 29 Encapsulated resist etching*

### *3.7 Nanopillar Fabrication*

Fabrication of silicon nanopillars on the template formed device is carried out in Micro-RIE. Formation of about 110nm silicon oxide pillar is carried out using gold as a mask in the etching. Single particle placement of DNA functionalized gold nanoparticles act as a mask during the etching process. Etch times and gas flow really do matter for the dimensions of the pillar and the grass formation on the substrate [48].

#### 3.7.1 Silicon oxide Reactive Ion Etching

We have used Plasma-Therm RIE for the etching of thermally deposited and plasma enhanced chemical vapor deposition of silicon oxide for the formation of nanopillars. The combination of oxygen and tetra fluorocarbon $CF_4$ were used for etching silicon nanostructures. This Plasma-Therm equipment was used as a PECVD later on it was modified as RIE. Top electrode has the connection RF power source which acts as cathode. We place our samples on the top electrode so as to have a selectivity of etching sample. RIE equipment chamber is 11-inch diameter which can have a gas flow of oxygen, tetrafluorocarbon, argon and SF6.

The etching chamber is cleaned to have a consistent result with silicon oxide etching. First step includes physical wet cleaning of chamber with mixture of isopropanol and DI water (3:1) with lint free wipes. This helps in removal of any particles in the chamber. Dry etching differs with any change in the chamber condition so, it's very important to carry out these wet cleaning process. In addition to wet clean, dry etching with oxygen plasma is carried out for 20 minutes to clean the polymer formation on the chamber. Later a conditioning step is performed to tune the equipment for the real process. This step is carried out for 15 minutes on a dummy wafer, later etching was performed on real sample.

Recipe used for anisotropic etching of silicon oxide is

CF4 -50 sccm
Pressure -80mTorr
Power – 200 W

Silicon oxide nanopillar with a height of 120nm is achieved for 12 minutes of etch time. The etch rate of silicon oxide is around 10nm per minute. The below SEM images shows anisotropic etch profile of silicon oxide. After formation of nanopillar Au nanoparticle is removed using wet gold etchant which comprises of potassium iodide and iodine. Au is removed because it cannot be used as hard mask in TRION DRIE equipment. Metal mask degrades the chamber condition during etching condition, to eliminate this, hard metal mask is not carried in DRIE etch chamber.

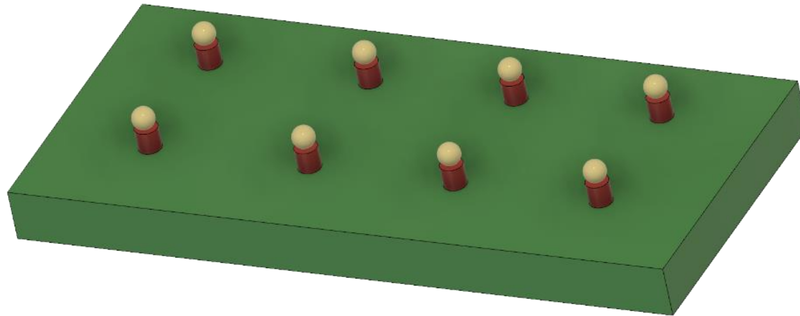

*Figure 30 Anisotropic etch of silicon oxide nanopillar using Au nanoparticle as hard mask*

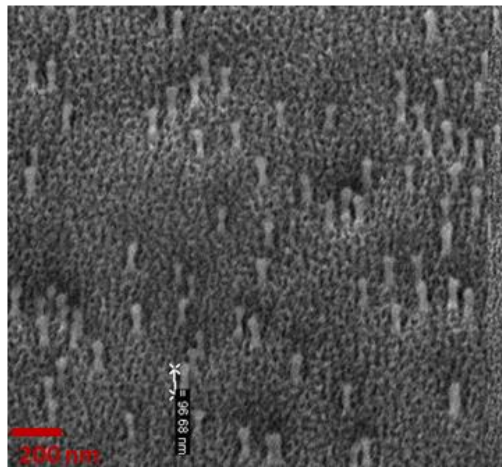


*Figure 31 PlasmaTherm RIE of silicon oxide for 12 minuates*

### 3.7.1 Anisotropic Silicon Etching

Anisotropic etching of silicon is carried out in TRION DRIE system with $CF_4$, helium and $O_2$ gas chemistry. Addition of helium gas assists in maintaining stable plasma during the etching process. Before carrying out the etching process, the main chamber is cleaned with oxygen plasma for ten minutes. Sample is placed on a carrier wafer and loaded into load lock chamber. This carrier wafer is loaded into main chamber with a robotic arm movement and placed on electrostatic chuck with a helium gas flow for cooling wafer. Helium base flow for cooling wafer is set at 4 sccm which has a lower leak rate less than 2 sccm. If higher leak rate is observed, sample is not

firmly attached to the chuck which varies the end result. Higher leak is usually observed when the carrier wafer is not clean or the chuck may be contaminated with particles.

The etched silicon oxide with Plasma-Therm RIE in the above SEM image shows rough surface which is due to polymer formation on the substrate. Substrate can be smoothening with ashing in oxygen plasma for 3 minutes with a flow of 100 sccm at 100W power in DRIE. Later etching of silicon is carried out to form a smoother finish on the substrate.

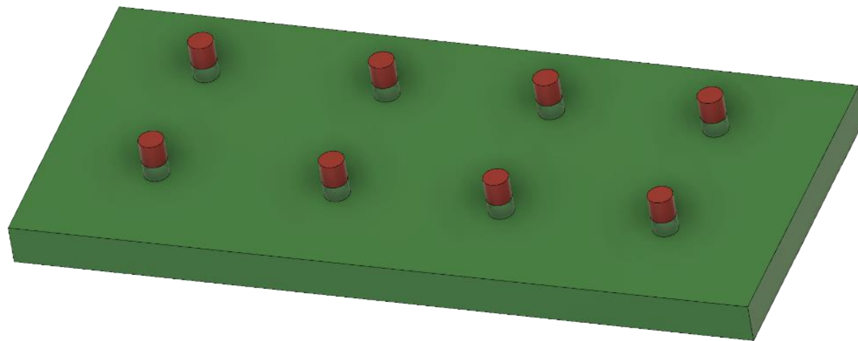

*Figure 32 Anisotropic silicon etch*

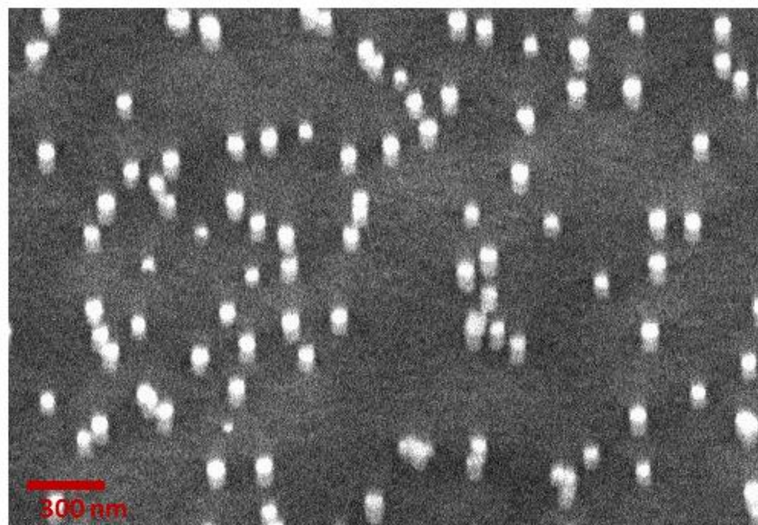


*Figure 33 Silicon and silicon oxide nanopillar*

The recipe used for etching silicon:

$CF_4$ – 35 sccm

$O_2$ -3 sccm

He – 50sccm

Pressure – 75mTorr

Power – 200 W

Etching of silicon is carried for 30 seconds to get a height of 70nm of silicon and 60 nm silicon oxide.

# Chapter 4
# Results and Discussion

## *4.1 Exposure dose*

An example of some of these process dependencies can be seen below which shows the effect of dose on a circular pattern. While the structures are well resolved at all five doses, the size of the final structures varies significantly.

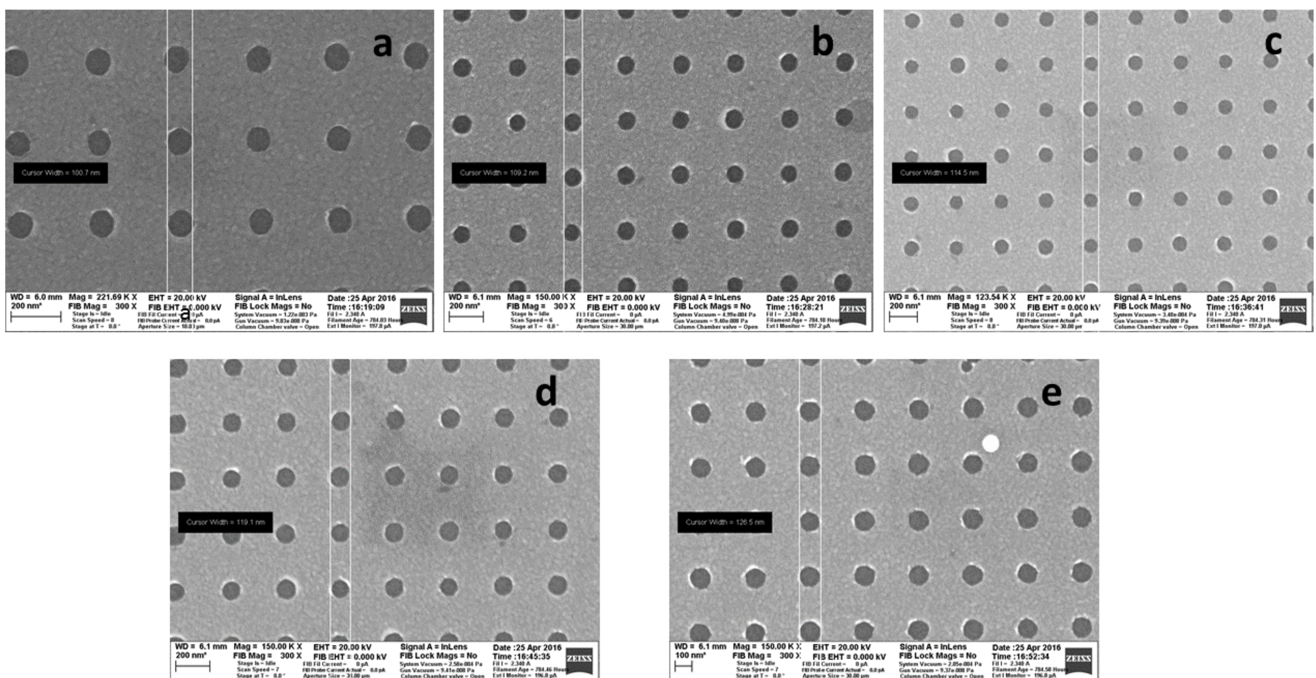


*Figure 34 SEM images with varied exposure dose (a) 130$\mu$C/cm$^2$ (b) 150 $\mu$C/cm$^2$ (c) 160 $\mu$C/cm$^2$ (d) 170 $\mu$C/cm$^2$ (e) 180 $\mu$C/cm$^2$*

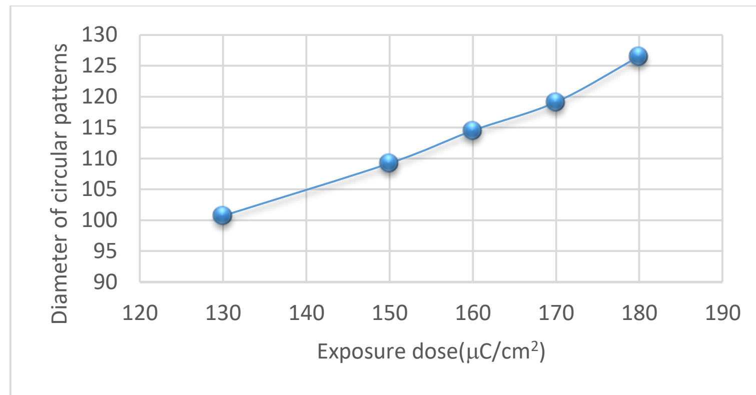


*Graph 1 Exposure dose vs circular diameter*

The electron beam is exposed on the spin-coated resist with varied exposure dose. SEM images were shown above with varied exposure dose on the resist substrate. The exposed sample is later subjected to development solution ma - D 525 for 10 seconds. Chrome and gold are deposited over the patterned sample and lift-off process is carried for 15 min to remove the resist on the surface.

### *4.2 Directed self-assisted Placement*

#### 4.2.1 Selectivity of Au nanoparticle placement

Fabrication of silicon oxide pattern is carried out using lithography and deposition techniques. The resulting pattern has surface gold and silicon oxide trench favoring the placement of DNA-functionalized Au nanoparticle with the assistance of SAM's layer formation on the exposed substrate. Formation of SAM's layer with APTES and MHA on the surface of silicon oxide and gold surface respectively. With the formation of SAM's layer results in a net positive and negative charge on the substrate when placed in ion concentration and pH controlled solution. To check the selectivity of attachment of Au nanoparticle on the substrate, a step formation of gold and silicon oxide surface is fabricated. The below SEM image shows a good selectivity of gold nanoparticle attachment to the silicon oxide substrate. Placement of 30nm gold in 1mM phosphate buffer solution with pH value 7.25.

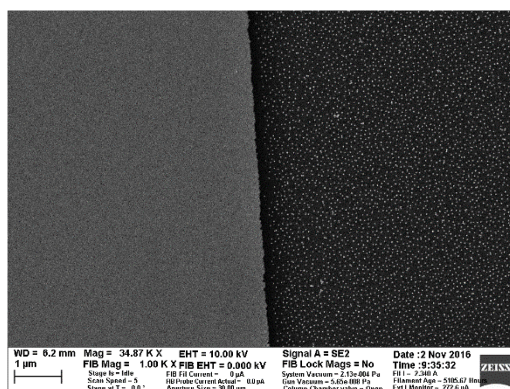


*Figure 35 Selective placement of 30nm Au on SiO2*

#### 4.2.2 Ion Concentration Effect

Ion concentration is the limiting factor for the particle double layer thickness. Higher ionic concentrations have excessive ions in the medium which get attracted towards the negative DNA functionalized Au nanoparticle thus degrading the charge of Au particle. In high ion concentration solution, thickness of the double layer becomes denser which screens the negative charge of the particle. Low ionic concentration has less screening effects which has higher negative charge on Au particle. This high negative charge experiences a greater repulsive forces from the gold surface which in turn having less number of Au nanoparticles attached on the silicon oxide holes.

The below SEM images shows the effect of different ion concentrations with constant pH 7. As you can see there's an increase in the number of Au nanoparticle attachment with an increase in ion concentration of the solution. For 0.1 mM PB solution number of single particle placement on silicon oxide is less compared to 0.5mM, 1mM and 10mM. Higher ionic concentration 10mM has a greater screening effect in the media which reduces the charge of Au particle which reduces repulsive forces from SAM's layer formed on gold surface. This results in attachment of more than one nanoparticle on the silicon oxide surface. Lower ionic concentration 0.1mM has low screening effect, means having higher negative charge of Au nanoparticle. Thus results with higher repulsive forces from SAM's layer on gold

surface. The number of Au nanoparticle attachment decreases due to higher repulsive forces from the surface.

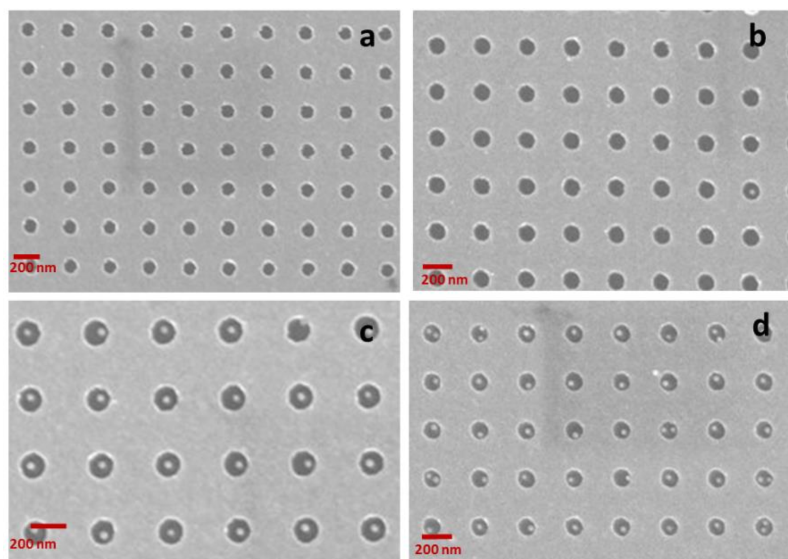


*Figure 36 Varied Ion concentration (Phosphate buffer solution) (a) 0.1mM (b) 0.5mM (c) 1mM (d) 10mM*

### 4.2.3 pH Effect

Single particle placement of functionalized Au nanoparticle placement on the substrate has noticeable effects on pH concentration of the solution during placement. When DNA is immersed in low pH solution, $[H^+]$ ion from the DNA hydrolysis is low compared to the ion concentration in the solution. Higher concentration of $[H^+]$ ion in the solution attach to the DNA and neutralize the particle charge. Functionalized gold nanoparticle placed in high pH solution $[H^+]$ ions of DNA react with $[OH^-]$ ions in the solution resulting in $H_2O$ generation. Various pH range were carried out to fin d out the Au placement in the silicon oxide trenches. These pH solutions were prepared with phosphate buffered solution which are made from monosodium phosphate and disodium phosphate in DI water.

Carboxylic acid terminated end formed during the SAM's layer formation dissociates into $COO^-$ and $H^+$ in water. When solution of pH increases $OH^-$ reacts to

form $H_2O$. Thereby increase in the negative charge on the Au surface with $COO^-$ terminated end.

Table 3 Mixtures of phosphate buffered solutions

| 1mM Phosphate buffer | $H_2NaO_4P \cdot H_2O$ (g/l) | $HNa_2O_4P \cdot 7\ H_2O$ (g/l) |
|---|---|---|
| pH 7.00 | 0.06 g | 0.15 g |
| pH 7.25 | 0.04 g | 0.19 g |
| pH 7.5 | 0.03 g | 0.22 g |

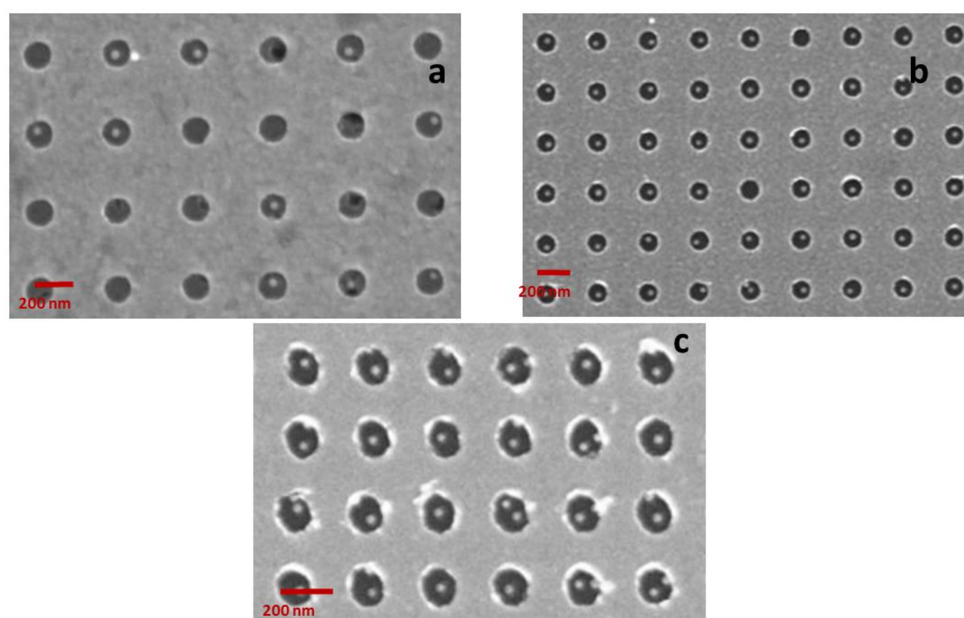


Figure 37 Effect of change in pH concentration of phosphate buffered solution (a) pH 7.0, (b) pH 7.25 and (c) pH 7.5

## 4.3 Resist Strip

Resist coating is carried out to protect the gold nanoparticle during the wet etching of gold and chromium substrate. E-beam resist ma-n 2401 is spin coated on the single particle placement sample, so that the hollow trenches and a thickness of 100 nm of resist id formed on the substrate. Now the resist is etched to the level of gold

surface, making sure the cylindrical holes are filled with resist. This etching is carried out by dry etching using Plasma-therm RIE. Oxygen chemistry is used for ashing out the resist on the substrate.

Before carrying it on real sample etch of the resist ashing is found out on a blanket silicon wafer. For this five samples were prepared to find out the etch rate. E-beam resist is spin coated on the blanket silicon wafer resulting a height of 1034 angstroms. Thickness of the resist is measured with ellipsometer with manufacture specified refractive index of the photo resist. The below table shows the final thickness of the resist after their etching.

*Table 4 Etch of resist*

| Sample | Initial Thickness (Å) | 4min etch (Å) | 5min etch (Å) | 6min Etch (Å) | 7min Etch (Å) | 8min Etch (Å) | Etch rate (Å) |
|---|---|---|---|---|---|---|---|
| 1 | 1040 | 568 | | | | | $(1040-568)/_4 = 118$ |
| 2 | 1045 | | 448 | | | | $(1045-448)/_5 = 119.4$ |
| 3 | 1034 | | | 330 | | | $(1034-330)/_6 = 117.34$ |
| 4 | 1050 | | | | 200 | | $(1050-200)/_7 = 121.42$ |
| 5 | 1038 | | | | | 80 | $(1038-80)/_8 = 119.75$ |

Average etch rate $= \frac{118+119.4+117.34+121.42+119.75}{5} = 119.18\ \text{Å}$

The etch was found to be almost 120 angstroms per minute. Using the above information, ashing was carried out on the real sample to expose the chrome substrate covering the cylindrical holes encapsulating Au nanoparticle with resist.

### *4.4 Selective Template removal*

Single particle placement of nanoparticle is studied above. Selective removal of chrome and gold deposited is done by wet etching using chrome and gold etchant. Au nanoparticle is protected with resist coating and the exposed surface is subjected to gold removal using gold etchant. Substrate is placed in gold etchant for 5 seconds

to remove all gold on the surface, which comprises of potassium iodide and iodine solution which etches at a rate of 28Å per second. Later sample is immersed in chrome etchant for 15 seconds to etch the chrome evaporated layer of thickness 50nm. Chrome etchant has an etch rate of 40Å per second, 3 seconds of over tech is carried out to remove all chrome surface. Resist which protects the gold nanoparticle is eliminated using oxygen plasma in Technics MicroRIE. The below SEM shows the Au nanoparticle at selective locations on the substrate.

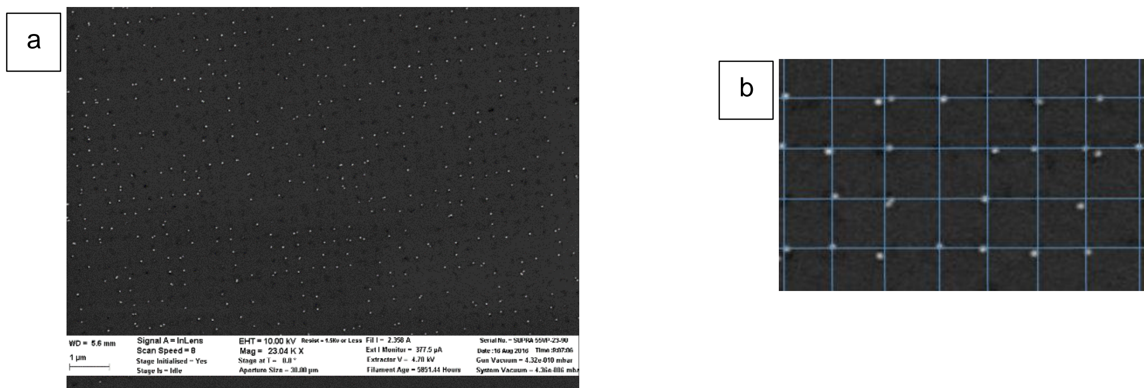


*Figure 38 Selective template removal with zoom in (a) and zoom out (b) SEM image*

### *4.5 Plasma-Therm RIE*

Etching of thermal deposition and plasma enhanced chemical vapor deposition of silicon oxide nanopillars is carried out on a blanket silicon wafer having only 30nm DNA-functionalized gold nanoparticle as hard mask. Placement of Au nanoparticle on blanket silicon oxide wafer with 1mM PB solution pH 7.0 gives a saturated placement over the surface. The sample is placed on the top electrode to have higher etch rate and anisotropic etching. This system is a modified version of PECVD where the top electrode is RF powered. Chamber is wet cleaned with a mixture of isopropanol and water and then oxygen plasma clean to remove the polymer layer formed on the chamber walls. To have consistent results with the equipment conditioning step is carried out before running a real sample for 30 minutes. Only $CF_4$ gas chemistry is used in etching silicon oxide.

Etching of thermally grown and plasma enhanced chemical vapor deposition of silicon oxide substrate is used to carry out fabrication of nanopillars. Nanopillars fabricated from plasma enhanced chemical vapor deposition of silicon oxide showed a poor adhesion. Falling of nanopillars is observed after dry etching of oxide layer using Au as hard mask. Later in the study, thermally grown silicon

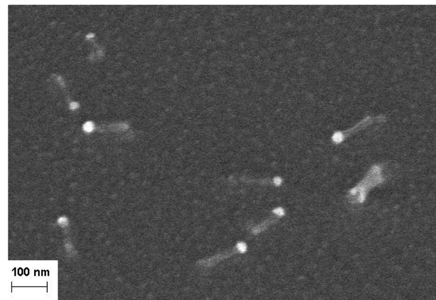


*Figure 39 PECVD of silicon oxide nanopillars*

Etching of thermally grown silicon oxide is carried out for 12 minutes leaving a height of 100nm. These SEM images were taken at an angle of 45°. The actual height is obtained by dividing with sin45° which comes to 117nm.

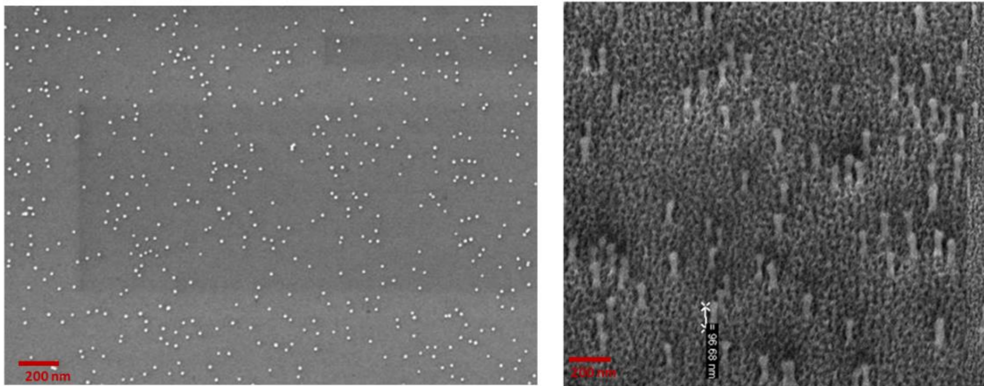


*Figure 40 Thermally deposited silicon oxide nanopillars (a) 30nm DNA-functionalized Au nanoparticle (b) 12 min etching*

### *4.6 DRIE etching*

DRIE etching is carried out in TRION etch systems to etch silicon having silicon oxide nanopillars on the substrate. Different etch recipes were carried out to find out

best etch recipe. Dry etching is dependent on many factors such as gas chemistry, gas flow, pressure, power and temperature of wafer. Different gas chemistry and pressures were carried out to find a suitable long silicon nanopillar.

$SF_6$ (14sccm) and $CHF_3$ (35sccm) chemistry was carried out in DRIE at 10mTorr pressure with 100W power. The resulting SEM seems to be rough which may be due to formation of polymer with the presence of $CHF_3$ gas in the chamber. Fluorine in $SF_6$ assists in etching silicon whereas $CHF_3$ helps in formation of polymer layer to the adjacent side walls to keep the profile of nanopillar straight.

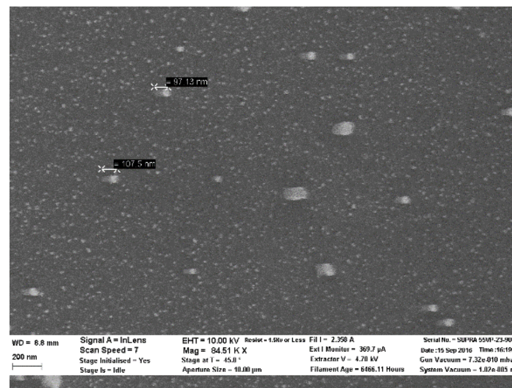


*Figure 41 Silicon/silicon oxide nanopillar with $SF_6$ and $CHF_3$ with TRION DRIE for 60seconds*

Secondly $CF_4$ (35sccm), He (50sccm) and $O_2$ (3sccm) chemistry was carried out with 75mTorr with 200W power. $CF_4$ is used to etch the silicon layer, addition of oxygen leads to increase on the Fluorine radicals which later increases the etch rate of silicon. Helium is added to the chamber to have a stable plasma. The SEM image was taken at an angle of 45°. The height of silicon/silicon oxide nanopillar was about 120nm (100/sin 45°). This chemistry is chosen to carry out the silicon etch due to its smooth finish.

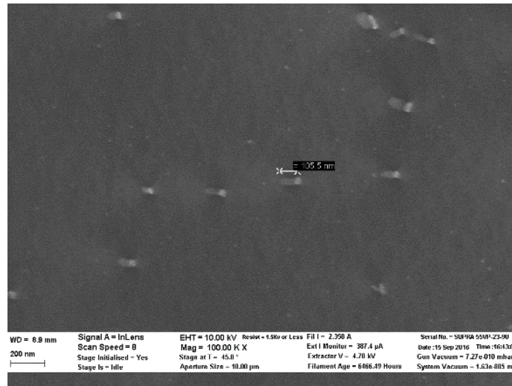

*Figure 42 Silicon/silicon oxide nanopillar with $CF_4$, He and $O_2$ with TRION DRIE for 60seconds*

$CHF_3$ (50sccm) and $SF_6$ (15sccm) gas chemistry is carried out later to find out the etch profile. 10mTorr pressure with 200W power is carried out. The substrate seems to be effected badly. This may be due to high gas flow of CHF3 when compared with the previous recipe.

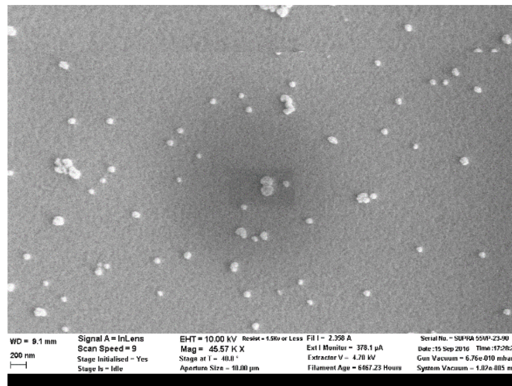

*Figure 43 Silicon/silicon oxide nanopillar with SF6 and CHF3 with TRION DRIE for 60seconds*

SF6 (30sccm) and O2 (16sccm) chemistry was carried out to eliminate the polymer formation in the previous recipe. Oxygen helps creating many F radicals and increases the etch of silicon. SEM image depicts a higher etching of silicon with a rough surface.

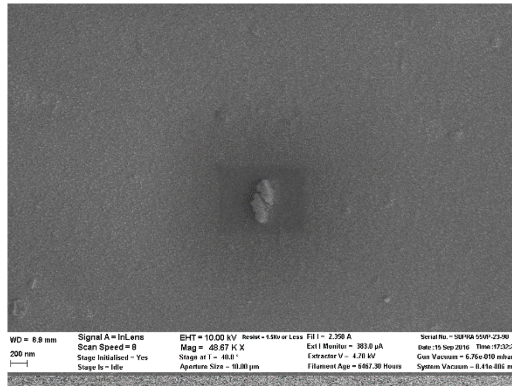


*Figure 44 Silicon/silicon oxide nanopillar with $SF_6$ and $O_2$ with TRION DRIE for 60seconds*

$CF_4$ (50sccm) is carried out to etch the silicon in the chamber. ICP is introduced to the top electrode to have a controllable plasma density which in turn increases the etch rate. 25mTorr pressure with 50W power to the lower electrode and 3000W ICP. The SEM image shows seriously damaged surface with this chemistry.

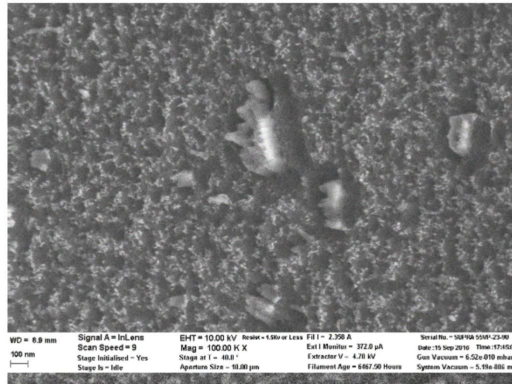


*Figure 45 Silicon/silicon oxide nanopillar with $CF_4$ with TRION DRIE for 60seconds*

From the above results $CF_4$, Helium and $O_2$ is best suited for anisotropic etching silicon. Having fixed with this chemistry effect of wafer cooling with Helium gas was carried out during dry etching in DRIE. Wafer was placed on an electrostatic chuck in the etching chamber. Helium gas flow of 5 sccm and 4 sccm was carried out and found out that leak rate was higher for a higher gas flow below the chuck which could not hold the wafer to the chuck firmly.

SEM images of two varied gas flows is shown below, image for 5 sccm helium gas flow shows a localized etching of silicon whereas for 4 sccm gas flow shows a smooth surface. The SEM image for 4 sccm is taken at an imperfection so as to get a focus on the substrate. Helium gas flow is generally used for cooling the wafer during the etching process. The temperature of electrons in plasma during etching is several thousand degrees, this, in turn, makes the substrate increase in temperature. To overcome this heating effect from plasma substrate is cooled with Helium gas flow below the wafer.

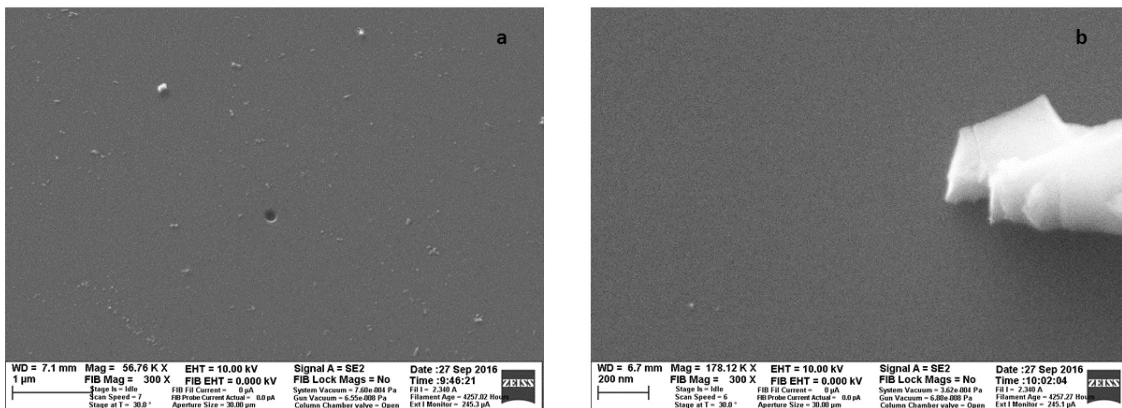


*Figure 46 Helium base flow (a) 5 sccm (b) 4 sccm*

Etch rate of the silicon is carried out by creating a step during etching. Later the step height was measured with KLA profilometer. A small silicon piece is taken and half part is covered with kapton tape which acts as a hard mask for the underlying silicon. $CF_4$, helium and $O_2$ recipe is carried out to measure the etch rate of silicon. Etching of silicon was carried out with 30 seconds with 200W power at 75mtorr pressure. Step height from the profilometer is found to be 1400Å for 30seconds etch in plasma. Etch rate of silicon was found to be 28nm per minute from the below profilometer readings.

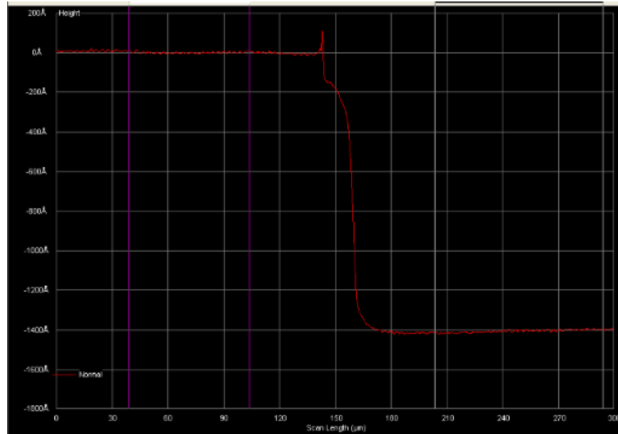


*Figure 47 Step height of silicon etch*

### *4.7 Buffered Oxide Etch*

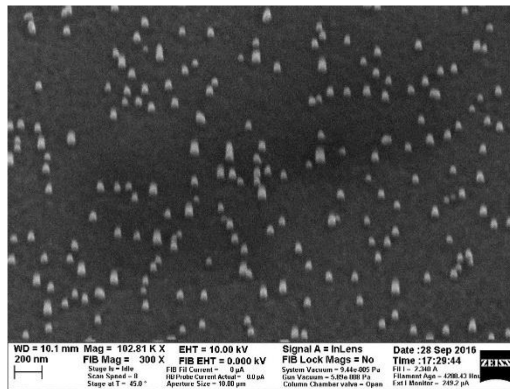


*Figure 48 Silicon nanopillar*

Trion DRIE equipment is used to carry out formation of silicon oxide/ silicon nanopillar. To accurately measure the height of the silicon nanopillar formed, silicon oxide nanopillar formed due to Plasma-Therm etch is wet etched with buffered oxide etching solution. Buffered oxide etch solution is a mixture of 40% ammonium fluoride and 49% hydrofluoric acid in the ratio of 6:1 (volume). Etch rate of silicon oxide varies depending on the deposition of oxide layers. On conducting experiments etch rate of thermally deposited silicon oxide is about 1.5nm per second. Fabricated silicon oxide /silicon nanopillar is placed in this solution for 2 minutes to etch silicon oxide pillar over

silicon. Sample is placed in the solution with extra seconds to make sure all the silicon oxide is etched. The below SEM image the silicon pillar with a height of about 70nm.

# Chapter 5
# Conclusion and Future Prospect

In this research, a novel approach for fabrication of single silicon/silicon oxide nanopillars at exact substrate positions has been investigated. In the process of achieving large-scale fabrication with precise placements of nanopillars, the following have been accomplished:

- Electrostatic guiding templates in which a gold layer contains 100 nm circular holes have been fabricated. The fabrication was accomplished by using E-beam lithography and deposition techniques. Variation of electron beam exposure during lithography was studied
- Selective functionalization of Au surface with negatively charged self-assembled monolayers and selective functionalization of $SiO_2$ surface with positively charged self-assembled monolayers have been accomplished. Au nanoparticles were functionalized with DNA. The electrostatic interactions between the SAMs-functionalized Au/$SiO_2$ surfaces and the DNA-functionalized Au nanoparticles led to placement of single Au nanoparticles on the centers of the circular holes. The electrostatic interactions were controlled by varying pH and ionic concentration of the solution.
- Selective removal of the gold template layer was accomplished in combination of controlled RIE of the resist and wet etching of Au layer, leaving well positioned Au nanoparticles on the substrate. Effects of different thicknesses of resist coatings for protecting AuNP were studied.
- For anisotropic silicon etching, different gas chemistries, powers, and pressures were investigated to obtain optimized RIE process. The

optimized process parameters for silicon nanopillar formation were found to be 35 SCCM $CF_4$, 3 SCCM $O_2$ and 50 SCCM He, 200W power, and 75 mTorr. The resultant nanopillars were 150nm in height and 30nm in diameter.

Although this thesis has demonstrated the formation of silicon and silicon oxide nanopillars on exact locations, the same approach could be used for formation of nanopillars/nanowires of other materials, e.g., silicon carbide nanowires. The capability of forming nanopillars on precise locations could find many applications in the areas of electronic/optical devices and chemical/biological sensors. In this thesis, development of single particle placement, selective template removal and fabrication of nanopillars were demonstrated on separate wafers. All these fabrication steps can be conducted on a single wafer to form nanopillars at exact substrate positions.

# References


[1] M. T. Björk, O. Hayden, H. Schmid1 and H. R. a. W. Riess, "Vertical surround-gated silicon nanowire impact ionization field-effect transistors," *Applied Physics Letters,* vol. 90, no. 14, 2007.

[2] T. Kamins, "Field effect transistor with gate layer and method of making same". United States of America Patent US20040097040 A1, 20 May 2004.

[3] T. J. Kempa, R. W. Day, S.-K. Kim and H.-G. P. a. C. M. Lieber, "Semiconductor nanowires: a platform for exploring limits and concepts for nano-enabled solar cells," *Energy & Environmental Science,* vol. 6, p. 719, 2013.

[4] M. T. e. al., "Silicon Nanwires: Fabrication and Applications," in *Anisotropic Nanomaterials*, Springer International Publishing Switzerland , 2015, pp. 1-25.

[5] C. S. Roper, A. Gutés, C. Carraro and R. T. H. a. R. Maboudian, "Single crystal silicon nanopillars, nanoneedles and nanoblades with precise positioning for massively parallel nanoscale device integration," *Nanotechnology,* vol. 23, no. 22, 2012.

[6] M. Elimelech and W. H. C. a. J. J. Waypa, " Measuring the zeta (electrokinetic) potential of reverse osmosis membranes by a streaming potential analyzer," *Desalination,* vol. 95, no. 3, pp. 296-286, 1994.

[7] R. J. Hunter, Zeta Potential in Colloid Science: Principles and Applications, Great Britan: Academic press, 1988.

[8] C. Z. I. a. D. Saville, "The interpretation of electrokinetic measurements using a dynamic model of the stern layer: I. The dynamic model," *Journal of Colloid and Interface Science,* vol. 114, no. 1, pp. 32-44, 1986.

[9] M. Fixman, "Thin double layer approximation for electrophoresis and dielectric response," *The Journal of Chemical Physics,* vol. 78, pp. 1483-1491, 1983.

[10] K. M, S. MP, M. PT, L. HF, D. JE and Lawrence Z and Kaiser C, "Approximate methods of determining the double-layer free energy of interaction," *Journal of Collid and Interface Science,* vol. 33, no. 3, pp. 335-359, 1970.

[11] D. A. Bryant, "Debye length in a kappa-distribution plasma," *Journal of Plasma,* vol. 56, no. 01, pp. 87-93, 1996.

[12] D. I. Klapper1, R. Hagstrom1, R. Fine2 and K. S. a. D. Barry, " Focusing of electric fields in the active site of Cu-Zn superoxide dismutase: Effects of ionic strength and amino-acid modification," *Proteins: Structure, Function, and Bioinformatics,* vol. 1, no. 1, pp. 47-59, 1986.

[13] R. Siden, DNA structure and function, London: Academic Press, 1994.

[14] M. Zheng, A. Jagota, M. S. Strano, A. P. Santos, P. Barone, S. G. Chou, B. A. Diner, M. S. Dresselhaus, R. S. Mclea, G. B. Onoa, G. G. Samsonidze, E. D. Semke and M. U. a. J. Walls, "Structure-Based Carbon Nanotube Sorting by Sequence-Dependent DNA Assembly," *Science,* vol. 302, no. 5650, pp. 1545-1548, 2003.

[15] D. Zanchet, C. M. Micheel, W. J. Parak and D. G. a. A. P. Alivisatos, "Electrophoretic Isolation of Discrete Au Nanocrystal/DNA Conjugates," *Nano Letters,* vol. 1, no. 1, 2001.

[16] Y. a. Z. G. Zu, "Facile and Controllable Loading of Single-Stranded DNA on gold Nanoparticles," *Analytical Chemistry,* vol. 81, no. 20, pp. 8523-8528, 2009.

[17] S. A. L.-J. a. C. M. Hurst, "Maximizing DNA loading on a range of gold nanoparticle sizes," *Analytical chemistry,* vol. 78, no. 24, pp. 8313-8318, 2006.

[18] L. M. Demers, C. A. Mirkin, R. C. Mucic, R. A. Reynolds, R. L. Letsinger and R. E. a. G. Viswanadham, "A Fluorescence-Based Method for Determining the Surface Coverage and Hybridization Efficiency of Thiol-Capped Oligonucleotides Bound to Gold Thin Films and Nanoparticles," *Analytical Chemistry,* vol. 72, no. 22, pp. 5535-5541, 2000.

[19] G. Timp, Nanotechnology, New York: Springer, 1999.

[20] A. A. Tseng, KuanChen and C. a. K. J. Ma, "Electron Beam Lithography in Nanoscale Fabrication: recent Development," *IEEE TRANSACTIONS ON ELECTRONICS PACKAGING MANUFACTURING,* vol. 26, no. 2, pp. 141-149, 2003.

[21] S. k. Ghandhi, VLSI Fabrication Principles: Silicon and Gallium Arsenide, New York: Wiley, 1994.

[22] A. Ulman, An Introduction to Ultrathin Organic Films, Boston: Academic Press, 1991.

[23] A. Ulman, "Formation and Structure of Self-Assembled Monolayers," *Chemical Reviews,* vol. 96, no. 4, pp. 1533-1554, 1996.

[24] J. C. Love, L. A. Estroff, J. K. Kriebel and R. G. N. a. G. M. Whitesides, "Self-assembled monolayers of thiolates on metals as a form of nanotechnology," *Chemical Reviews,* vol. 105, no. 4, pp. 1103-1170, 2005.

[25] C. Vericat, M. E. Vela, G. Corthey, E. Pensa, E. Cortes, M. H. Fonticelli, F. Ibanez, G. E. Benitez and P. C. a. R. C. Salvarezza, "Self-assembled monolayers of thiolates on metals: a review article on sulfur-metal chemistry and surface structures," *RSC Advances,* vol. 4, pp. 27730-27754, 2014.

[26] D. K. Schwartz, "MECHANISMS AND KINETICS OF SELF-ASSEMBLED MONOLAYER FORMATION," *Physical Chemistry,* vol. 52, pp. 107-137, 2001.

[27] S. A. Jadhav, "Self-assembled monolayers (SAMs)," *Central European Journal of Chemistry,* vol. 9(3), pp. 369-378, 2011.

[28] J. C. Love, L. A. Estroff, J. K. Kriebel, R. G. Nuzzo and G. M. Whitesides, "Self-Assembled Monolayers of Thiolates on Metals as a Form of Nanotechnology," *Chemical Reviews,* vol. 105, pp. 1103-1169, 2005.

[29] N. Faucheuxa, R. Schweiss, K. Lutzow, C. Werner and T. Groth, "Self-assembled monolayers with different terminating groups as model substrates for cell adhesion studies," *Biomaterials,* vol. 25, pp. 2721-2730, 2004.

[30] R. G. Acres, A. V. Ellis, J. Alvino, C. E. Lenahan, D. A. Khodakov, G. F. Metha and G. G. Andersson, "Molecular Structure of 3-Aminopropyltriethoxysilane Layers Formed on Silanol-Terminated Silicon Surfaces," *Physical Chemistry,* vol. 116, pp. 6289-6297, 2012.

[31] A. Mohammed, R. A. Rahim, I. J. Ibraheem, F. K. Loong, H. Hisham and U. H. a. Y. Al-Douri, "Application of Gold Nanoparticles for Electrochemical DNA Biosensor," *Journal of Nanomaterials,* 2014.

[32] R. G. Acres, A. V. Ellis, J. Alvino, C. E. Lenahan, D. A. Khodakov and G. F. M. a. G. G. Andersson, "Molecular Structure of 3-Aminopropyltriethoxysilane Layers Formed on Silanol-Terminated Silicon Surfaces," *The Journal of Physical Chemistry,* vol. 116, no. 10, pp. 6289-6297, 2012.

[33] M. B. Haddada, J. Blanchard, S. Casale, J.-M. Krafft, A. Vallée, C. Méthivier and S. Boujday, "Optimizing the immobilization of gold nanoparticles on functionalized silicon surfaces: amine- vs thiol-terminated silane," *Gold Bulletin,* vol. 46, no. 4, pp. 335-341, 2013.

[34] H. H. Kyaw, S. H. Al-Harthi and A. S. a. J. Dutta, "Self-organization of gold nanoparticles on silanated surfaces," *Beilstein Journal of Nanotechnology,* vol. 6, pp. 2345-2353, 2015.

[35] R. G. NUZZO, B. R. Zegarski and L. H. Dubois, "Fundamental Studies of the Chemisorption of Organosulfur Compounds on Au( 11 1). Implications for Molecular Self-Assembly on Gold Surfaces," *Journal of the American Chemical Society,* vol. 109, pp. 733-740, 1987.

[36] C. D. Bain, E. Barry, Y.-T. Tao, J. Evall, G. M. Whitesides and R. G. Nuzzo, "Formation of Monolayer Films by the Spontaneous Assembly of Organic Thiols from Solution onto Gold," *Journal of the American Chemical Society,* vol. 111, pp. 321-335, 1989.

[37] Madprime, 2016. [Online]. Available: https://en.wikipedia.org/wiki/DNA. [Accessed 13 June 2016].

[38] S. J. Hurst and A. K. R. L.-J. a. C. A. Mirkin, "Maximizing DNA Loading on a Range of Gold Nanoparticle Sizes," *Analytical Chemistry,* vol. 78, no. 24, pp. 8313-8318, 2006.

[39] Y. Z. a. Z. Gao, "Facile and Controllable Loading of Single-Stranded DNA on Gold Nanoparticles," *Analytical Chemistry,* vol. 81, no. 20, pp. 8523-8528, 2009.

[40] H. D. Hill, J. E. Millstone and M. J. B. a. C. A. Mirkin, "The Role Radius of Curvature Plays in Thiolated Oligonucleotide Loading on Gold Nanoparticles," *ACS Nano,* vol. 3, no. 2, pp. 418-424, 2009.

[41] D. LM, M. CA, M. RC, R. RA, L. RL and E. R. a. G, "A fluorescence-based method for determining the surface coverage and hybridization efficiency of thiol-capped oligonucleotides bound to gold thin films and nanoparticles," *Analytical Chemistry,* vol. 72, no. 22, pp. 5535-5541, 2000.

[42] K.-S. H, P. DY and T. M. a. W. LJ, "Base-dependent competitive adsorption of single-stranded DNA on gold.," *Journal of American Chemical Society,* vol. 125, no. 30, pp. 9014-9015, 2003.

[43] L.-C. Ma, R. Subramanian, H.-W. Huang, V. Ray, C.-U. Kim and S. J. Koh, "Electrostatic Funneling for Precise Nanoparticle Placement: A Route to Wafer-Scale Integration," *Nano Letters,* vol. 7, no. 2, pp. 439-445, 2007.

[44] K. Nojiri, Dry Etching Technology for Semiconductors, Springer, 2014.

[45] K. Nojiri, Dry etching technology fro semi conductors, Springer International Publishing, 2015.

[46] "GE life sciences," April 2007. [Online]. Available: https://www.gelifesciences.com/gehcls_images/GELS/Related%20Content/Files/1314774443672/litdoc17085301_20161014154720.pdf. [Accessed 7 November 2016].

[47] [Online]. Available: https://www.cureuv.com/products/uva-lamp-total-cure-power-shot-500?variant=24246846087.

[48] P. A. Lewis, H. Ahmed and T. Sato, "Silicon nanopillars formed with gold colloidal particle masking," *Journal of Vacuum scienc & technology B,* vol. 16, p. 2938, 1198.

[49] I. Cornago, A. L. Hernández, R. Casquel, M. Holgado, M. F. Laguna and F. J. S. a. J. Bravo, "Bulk sensing performance comparison between silicon dioxide and resonant high aspect ratio nanopillars arrays fabricated by means of interference lithography," *OPTICAL MATERIALS EXPRESS,* vol. 6, no. 7, 2016.

[50] I. Cornago, A. L. Hernández, R. Casquel, M. Holgado, M. F. Laguna and F. J. S. a. j.Bravo, "Bulk sensing performance comparison between silicon dioxide and resonant high aspect ratio nanopillars arrays fabricated by means of interference lithography," *OPTICAL MATERIALS EXPRESS,* vol. 6, no. 7, 2016.

[51] V. k. a. H.-F. Ji, "Nanopillars for Sensing," *Journal of Nanoscience and Nanotechnology,* vol. 14, no. 9, pp. 6469-6477, 2014.

[52] B. D. Choudhury, R. Casquel, M. Bañuls, F. Sanza, M. Laguna, M. Holgado, R. Puchades, A. Maquieira and C. B. a. S. Anand, "Silicon nanopillar arrays with SiO2 overlayer for biosensing application," *Optical Materials Express,* vol. 4, no. 7, pp. 1345-1354, 2014.

[53] J. Choi, T. S. Lee, D. S. Jeong, W. S. Lee, W. M. Kim, K.-S. Lee and D. K. a. I. Kim, "Random Si nanopillars for broadband antireflection in crystalline silicon solar cells," *Journal of Physics D: Applied Physics,* vol. 49, no. 37, 2016.

[54] Z. Li, Y. Chen, X. Zhu1, M. Zheng, F. Dong, P. Chen, L. Xu and W. C. a. H. Duan, "Fabrication of single-crystal silicon nanotubes with sub-10-nm walls using cryogenic inductively coupled plasma reactive ion etching," *Nanotechnology,* vol. 27, no. 36, 2016.